Journal of Hydrology 428–429 (2012) 32–50

Contents lists available at SciVerse ScienceDirect

Journal of Hydrology

journal homepage: www.elsevier.com/locate/jhydrol

Integrating topography, hydrology and rock structure in weathering rate models of spring watersheds

Fernando A.L. Pacheco [a,*], Cornelis H. Van der Weijden [b,1]

[a] Department of Geology & Centre for Chemistry, Trás-os-Montes and Alto Douro University, Ap 1013, 5000 Vila Real, Portugal
[b] Department of Earth Sciences—Geochemistry, Faculty of Geosciences, Utrecht University, P.O. Box 80.021, 3508 TA, Utrecht, The Netherlands

ARTICLE INFO

Article history:
Received 7 April 2011
Received in revised form 22 November 2011
Accepted 18 January 2012
Available online 30 January 2012
This manuscript was handled by Philippe Baveye, Editor-in-Chief

Keywords:
Spring watersheds
Hydrology
Travel time
Surface area
Weathering rates
Modeling

SUMMARY

Weathering rate models designed for watersheds combine chemical data of discharging waters with morphologic and hydrologic parameters of the catchments. At the spring watershed scale, evaluation of morphologic parameters is subjective due to difficulties in conceiving the catchment geometry. Besides, when springs emerge from crystalline massifs, rock structure must be accounted in formulas describing the area of minerals exposed to the percolating fluids, for a realistic evaluation of the rates. These particular features are not included in the available approaches and for that reason a new model was developed, coined THROW model. This is a lumped approach that integrates (T)opography, (H)ydrology, (RO)ck structure and (W)eathering in a single algorithm. The study area comprises several stream watersheds and spring sites of the Vouga River basin (northern Portugal), shaped on granites. Firstly, the THROW model couples a terrain modeling analysis with hydrologic models based on discharge rates, to determine hydraulic conductivities (K), effective porosities (n_e) and annual recharges (V_r) at the stream watershed scale. Subsequently, these parameters are used in a water balance model to estimate concomitant groundwater travel times (t). The mean K [$(4.7 \pm 3.2) \times 10^{-7}$ m s^{-1}] and n_e [$(2.0 \pm 1.3) \times 10^{-2}$] values are adopted as proxies for the spring watersheds and a firm regression equation is defined between time and stream watershed area (A). Secondly, two more runs of terrain modeling analysis are executed to extrapolate morphologic parameters for the spring watersheds. The first run hinges on scaling properties of the drainage networks, known as Horton laws, and is used to scale watershed areas across stream orders (i). The scaling function is described by another regression equation. The second run evaluates the order of a spring watershed, defined as equivalent order (i_{eq}) and equated to the mean order of the surrounding stream watersheds. Having calculated the i_{eq}, spring watershed areas and travel times were downscaled using the regression equations (A < 10 km^2 and t = 1.4–2.8 year). Standing on the physical and hydrologic parameters of the spring watersheds, the THROW model finally calculates plagioclase weathering rates in the vicinity of the spring sites. The SiB model (Pacheco and Van der Weijden, 1996) was used before to estimate the contribution of plagioclase dissolution to the chemical composition of these springs (Van der Weijden and Pacheco, 2006). The chemical data were now coupled with K, n_e and t in a rate equation to estimate chemical weathering rates of plagioclase in the basin. In the THROW model, the rate equation describes the exposed surface area as a function of fracture spacings, openings and porosities (Pacheco and Alencoão, 2006). The calculated rates (W_{Pl} = $(2.5 \pm 1.2) \times 10^{-14}$ mol m^{-2} s^{-1}) are consistent with previous reports and with results of experimental kinetic models. The SiB results predict formation of halloysite and gibbsite along the flow path, which were indeed close to equilibrium with the dissolved Al and Si activities.

© 2012 Elsevier B.V. All rights reserved.

1. Introduction

The assessment of chemical weathering rates of silicate minerals has been the topic of numerous studies, as this process is important in global geochemical cycles, particularly in relation to fluxes of carbon dioxide (CO_2) and global warming (Berner et al., 1983; Drever and Clow, 1995; Dupré et al., 2003; Hartmann et al., 2009; among others). These studies have been carried out at various scales, including the micro to hand specimen scales (the laboratory approach) or the soil profile to watershed scales (the field approach). At the watershed scale, the majority of studies were focused on rivers (Oliva et al., 2003; Tardy et al., 2004; Velbel, 1985; White, 2002; White et al., 2001; and references therein) while a limited number were based on spring water data (Pacheco and Van der Weijden, 2002; Pacheco and Alencoão, 2006). Studies at the spring watershed scale are important because they bridge weathering results from the hand specimen or soil profile to the

* Corresponding author. Fax: +351 259 350480.
E-mail addresses: FPACHECO@UTAD.PT (F.A.L. Pacheco), CHVDW@GEO.UU.NL (C.H. Van der Weijden).
[1] Fax: +31 30 2535302.

0022-1694/$ - see front matter © 2012 Elsevier B.V. All rights reserved.
doi:10.1016/j.jhydrol.2012.01.019

river basin scales. Numerical models have been developed and applied to calculate weathering rates. At the watershed scale, operation of these models requires prior assessment of very diverse data, such as morphologic parameters of the catchments, aquifer hydraulic parameters and recharge, groundwater travel times, fluid compositions, etc., incoming from very different disciplines, including geomorphology, hydrology or geochemistry, reason why the most recent models are based on the so-called lumped approach, whereby the results of several model components are integrated. For example, Goddéris et al. (2006) combined a module of chemical weathering in soil horizons and underlying bedrock (the WITCH model of Goddéris et al., 2006, 2009; Roelandt et al., 2010) with a module of water and carbon cycles in forested ecosystems (the ASPECTS model of Rasse et al., 2001) to simulate, on a seasonal basis, the concentrations of silica and major base cations within the soil horizons and the stream of a granitic small experimental watershed. Violette et al. (2010) designed two symmetrical box modules to perform a coupled hydrological and geochemical modeling: (i) a hydrological module specifically developed for the experimental watershed; (ii) the WITCH module. The hydrologic modules commonly incorporated into lumped approaches are usually designed to work with stream watersheds, and the concomitant geochemical modules relate the fluid compositions to weathering reactions in the saprolite horizon and quantify the area of minerals involved in weathering reactions (the exposed surface area) as a function of the saprolite materials texture (e.g. Violette et al., 2010). Despite their broad applicability, available lumped approaches are inoperative when the study is focused on springs emerging from crystalline rocks, because they cannot accommodate some singularities of fracture artesian spring watersheds relative to geometry and exposed surface area. For that reason, a new approach is required to deal with such cases.

A lumped approach suited to deal with fracture artesian springs must incorporate a topographic module that can assess watershed morphologic parameters (area, volume, length of water channels), yet recognizing that spring sites can hardly be connected to a water channel. This type of springs emerges at the intersection between the Earth's surface and conductive fractures. Usually, this corresponds to points in the vicinity of water channels but rarely to points in a specific channel. In these cases, delineation of watershed boundaries becomes a subjective task that limits any subsequent morphologic characterization. An appropriate topographic module has to calculate the morphologic parameters avoiding the step of watershed delineation, however such a specific method is not part of any current lumped approach. Additionally, the lumped approach must also bear that fracture artesian springs represent water packets that predominantly follow the easiest routes of the crystalline rocks, such as fissures, fractures or joints, interacting with minerals exposed at their walls. The area of fluid–mineral interaction is not equal to the area of the catchment, but is restricted by inhomogeneous fluid migration through the fracture networks (Drever and Clow, 1995; Velbel, 1989, 1993). Moreover, minerals in the fractures are generally embedded in the rock matrix and are only partly exposed to the fluid. Along the pathway from recharge area to spring site, a water packet has been in contact with mineral surfaces that have different weathering histories. For this reason, the exposed surface area will be an average of newly exposed minerals and of minerals already affected by weathering. Furthermore, the spring water samples represent combined water packets, each having traveled different pathways with various contact times and exposure to different surface areas (Oliva et al., 2003). As a consequence, the calculated weathering rate will represent an average. For the reasons described above, the geochemical module of the lumped approach should define the exposed surface area as a function of rock structure, whenever the studied watersheds are shaped on crystalline rocks and the analyzed water samples are represented by groundwater. Nevertheless, this is not observed in the available models. Invariably, this area is calculated from the crystal dimensions of the minerals (geometric surface area) or by gas adsorption (BET method) that accounts for the so-called surface roughness (Brantley et al., 1999; Brantley and Mellott, 2000; Lüttge 2005; Zhang and Lüttge, 2009), although it has already been recognized that the results might not be representative of the area exposed to groundwater in a watershed (Brantley and Mellott, 2000; Drever and Clow, 1995; Hellmann and Tisserand, 2006; White and Peterson, 1990a,b).

The present study sought to calculate weathering rates of plagioclase at the spring watershed scale in granitic environment. Given the above mentioned singularities of fracture artesian spring watersheds, the main purpose of this paper is to develop a lumped approach integrating, (a) a topographic module that can estimate the morphologic parameters of the spring watersheds; (b) a geochemical module that defines the exposed surface area as a function of rock structure. The lumped approach will be coined as the (T)opography, (H)ydrology, (RO)ck structure and (W)eathering model, or simply THROW model. The module developed for assessing the spring watershed morphologic parameters is based on the concepts of stream order (Strahler, 1957) and statistical self-similarity of drainage networks (Horton, 1945; Schuller et al., 2001). In an attempt to account for the particularities of fluid transport in fractured rocks as described above, the area of fluid–mineral interaction will be approximated in the geochemical module by a formula hinging on rock fracture spacings, openings and porosities (Snow, 1968; Pacheco and Alencoão, 2006).

2. Study area

The hydrographic basin of the Vouga (Fig. 1) is located in northern Portugal between the sea level of the Atlantic coast and 1100 meters above sea level, near the source of the river on Lapa Mountain. The basin occupies 3362 km^2 of a region characterized by mountains in the eastern part and a coastal plain in the western part. Altitudes in major mountains (Lapa, Freita, Caramulo) range from 800 and 1100 meters. The main water course is 141 km long and debouches into the Ria de Aveiro, a sandbar-built coastal lagoon with a small inlet/outlet connecting the lagoon to the Atlantic ocean. The climate in this region is moderate, with precipitation varying from 800–1800 $mm \cdot y^{-1}$ and air temperatures ranging from approximately 8 °C in winter to 21 °C in summer. The Vouga River and several tributaries have been monitored for stream flow in hydrometric stations of the Portuguese National Network. The locations of the stations are shown in Fig. 1 and some relevant data on identification and record length is presented in Table 1.

The mountainous part of the Vouga River basin is characterized by Palaeozoic metasediments of the so-called Schist and Greywacke Complex (Beiras Group) that were intruded by syn- to post-tectonic Hercynian granites. The coastal plain has a cover of Permian to Holocene sediments consisting of quartzites, phyllites, conglomerates, sandstones, limestones, sands, etc. (Fig. 2). The syntectonic granitoids consist mostly of medium- to coarse-grained granites to granodiorites, whereas the post-tectonic granitoids consist mostly of coarsely porphyritic biotite granites (Schermerhorn, 1956; Soen, 1958; Godinho, 1980; Medina, 1996). The average mineralogical composition (in wt.%) of these rocks is: quartz (34.1), *K*-feldspar (14.4), plagioclase (albite-oligoclase, but largely oligoclase; 31.0), biotite (3.7), and muscovite (16.8).

The mountainous part of the Vouga basin has a monotonous cover by cambisols. In the plain, soil types are dominated by fluvisols, regosols, podzols and solonchaks. In the region, the profile of a typical cambisol is characetrized by an A horizon (0–30 cm depth) rich in organic matter, a B horizon (30–55) rich in clay minerals and a C

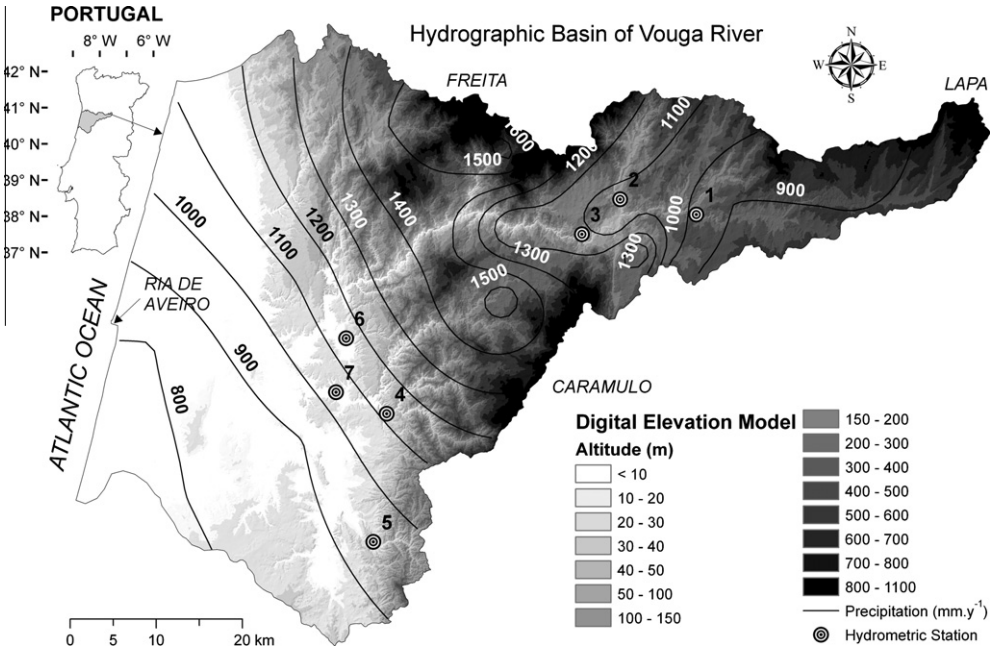

Fig. 1. Location of Vouga river basin in the North of Portugal and next to the Atlantic Ocean. Digital Elevation Model (DEM) of the basin with reference to surrounding mountains (Lapa, Caramulo and Freita) and to the mouth area in the Ria de Aveiro. Distribution of precipitation (P) and of hydrometric stations (labeled circles) inside the basin. The labels of the circles agree with the Id numbers in Table 1.

Table 1
Morphologic and hydrologic characterization of seven watersheds within the Vouga River hydrographic basin. Id – Label of the hydrometric station located at the outlet of the watershed, in agreement with labels in Fig. 1; Code – identification of code of the hydrometric station; X, Y – location coordinates of the hydrometric station, in the Hayford-Gauss system; V, A and L – volume and area of the watershed and length of water channels within the watershed; a_1, a_3 – intercept-y of the dashed lines in Fig. 7; K, n_e – average hydraulic conductivity and effective porosity of the watershed; Q_i, Q_f – average base flow discharge rates at the start and end of recession periods; V_r – average annual recharge; t – average groundwater travel time. The average values pertain to the record length of each station.

Parameter	Units	Value						
Id		1	2	3	4	5	6	7
Code		09 J/01	09I/03	09I/02	10G/05	11G/01	10G/01	10G/02
River		Vouga	Sul	Vouga	Águeda	Serra	Marnel	Águeda
Starting year		1936	1981	1917	1977	1978	1977	1934
Record length	year	17	9	40	12	11	10	52
X	m	15,086	6238	1797	−20,880	−22,428	−25,588	−26,764
Y	m	121,045	122,825	118,766	97,871	82,965	106,651	100,372
$V \times 10^9$	m^3	71	62	317	82	12	7	236
$A \times 10^6$	m^2	274	110	649	152	40	22	405
$L \times 10^3$	m	177	59	146	79	39	24	138
$a_1 \times 10^{-9}$		3.4	8.4	2.1	25.1	75.4	33.9	9.2
$a_3 \times 10^{-11}$		16.9	92.6	1.4	27.9	2272.0	1020.9	0.8
$K \times 10^{-7}$	$m\ s^{-1}$	2.4	1.7	8.4	4.2	2.7	2.8	10.7
$n_e \times 10^{-2}$		3.7	1.1	3.7	0.9	0.4	1.5	3.0
Q_i	$m^3\ s^{-1}$	15.42	7.75	30.0	12.5	2.0	3.2	30.0
Q_f	$m^3\ s^{-1}$	0.18	0.19	1.0	0.175	0.05	0.01	1.2
$V_r \times 10^6$	m^3	57	28	109	46	7	12	108
t	year	46	25	107	16	7	9	66

horizon (55–80) composed of weathered rock (Martins, 1985). Average hydraulic conductivity of this soil type is $K = 2.47 \times 10^{-6}$ m s^{-1} (Caetano and Pacheco, 2008). When 1D flow is assumed, percolation time of soil water to the bedrock (h/K, where h = 80 cm, the average thickness of cambisols) is at least 3.75 days. Small-size farm lands and forests in total occupy 4/5 of the basin, the remaining 1/5 being represented by bare rock, urban areas and water bodies. Although farming is more concentrated in the plain and forestry in the mountains, the proportion of land used for agriculture in the highlands is significant and the associated use of manure and fertilizers responsible for an important anthropogenic imprint to the chemistry of shallow groundwaters. Some small urban areas have no sewage system and so domestic effluents are discharged directly into the soils (Van der Weijden and Pacheco, 2006).

3. Spring water sampling and analytical techniques

Perennial springs within the Vouga basin were sampled in the granitic areas during the summer campaigns (June–July) of 1982–1985. In total, the number of sampled springs is 87. The location of the spring sites is given in Fig. 2. Sampling was made during the draught season to ensure that spring waters would represent exclusively ground water. The pH was measured at the sampling site, and alkalinity was analyzed in the field laboratory within 24 h of sample collection using Gran plots for end-point determination. Two samples of 100-mL each, one acidified with nitric acid to pH 2, were stored and analyzed at the home laboratory. Sodium, potassium, magnesium, calcium, aluminum, and silicon were analyzed by ICP-OES in the acidified sample, whereas chloride,

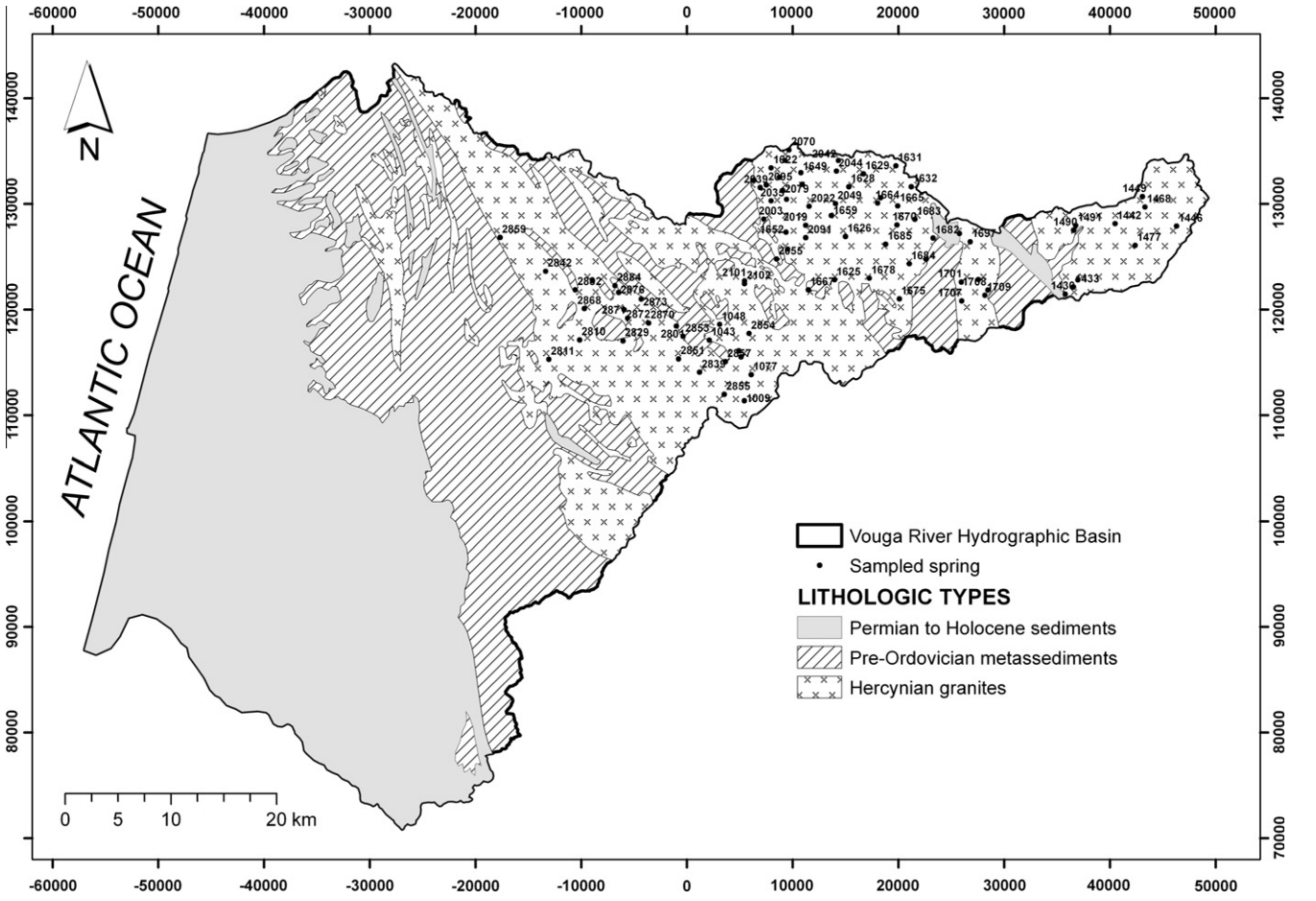

Fig. 2. Simplified geological map of Vouga river basin. Adapted from the Geological Map of Portugal, scale 1/500,000, produced in 1992 by the Portuguese Geological Survey. Distribution of the sampled springs (labeled black dots) within the granite area of the basin. The labels of the dots agree with Sample # in Appendix A.

sulfate, and nitrate were determined by ion chromatography in the unacidified sample. The accuracy of the results for the individual components was better than ± 5%. Samples for which the charge balance was off by > 10% were discarded. The analytical results are reported in Appendix A.

4. The throw model

The THROW model is introduced in this paper as a lumped approach for the assessment of weathering rates at the fracture artesian spring watershed scale. It is composed of three modules: the topographic module, the hydrologic module and the weathering module. A run of the THROW model begins with the topographic module, proceeds with the hydrologic module and ends up with the weathering module, as illustrated in the flowchart of Fig. 3. Each module is organized within the dashed envelopes of the figure: the rectangles represent data essential for model operation; the rounded rectangles represent model processes. Because the THROW model runs in a sequential mode, the output of a given process is usually the input for the next process, until weathering rates are finally calculated. The shaded rectangles, however, represent base information, obtained from topographic, analytical or field measurements. The description of the topographic, hydrologic and weathering modules is presented in the next sections.

4.1. The topographic module

The topographic module of the THROW model aims on estimating morphologic parameters (e.g. area) of spring watersheds. There is a fundamental difficulty in dealing with these watersheds because springs typically emerge in the vicinity of several water channels but not necessarily in any channel. As a consequence, the outlining of spring watersheds is a biased task that hampers any subsequent morphologic characterization. For that reason, morphologic parameters of spring watersheds in the THROW model are estimated by an extrapolation technique based on scaling properties of the drainage networks.

4.1.1. The horton laws of drainage network composition

The continuous shaping of the Earth's surface by meteoric water results in the development of drainage networks that can be conceived at various scales: river, stream, spring. Scaling properties of drainage networks were early investigated and empirical scaling laws have been proposed by Horton (1945), Strahler (1952) and Schumm (1956), becoming known as the Horton laws. Subsequent research has shown that individual streams and the networks which they comprise are fractals (La Barbera and Rosso, 1987, 1989; Roth et al., 1996; Tarboton, 1996; Schuller et al., 2001; De Bartolo et al., 2006; among others), and the Horton laws provided the background for the development of different measures of the fractal dimension. These empirical rating laws are based upon hierarchical classification of the tributary system starting from streams lacking upstream tributaries and giving increasing order numbers towards the outlet. For example, according to the classification of Strahler (1957), water channels with no tributaries are described as 1st-order channels and are fed by 1st-order watersheds, and the confluence of two ith-order channels generates a $(i + 1)$th-order channel. Basically, the scaling laws state that the ratio of a morpho-

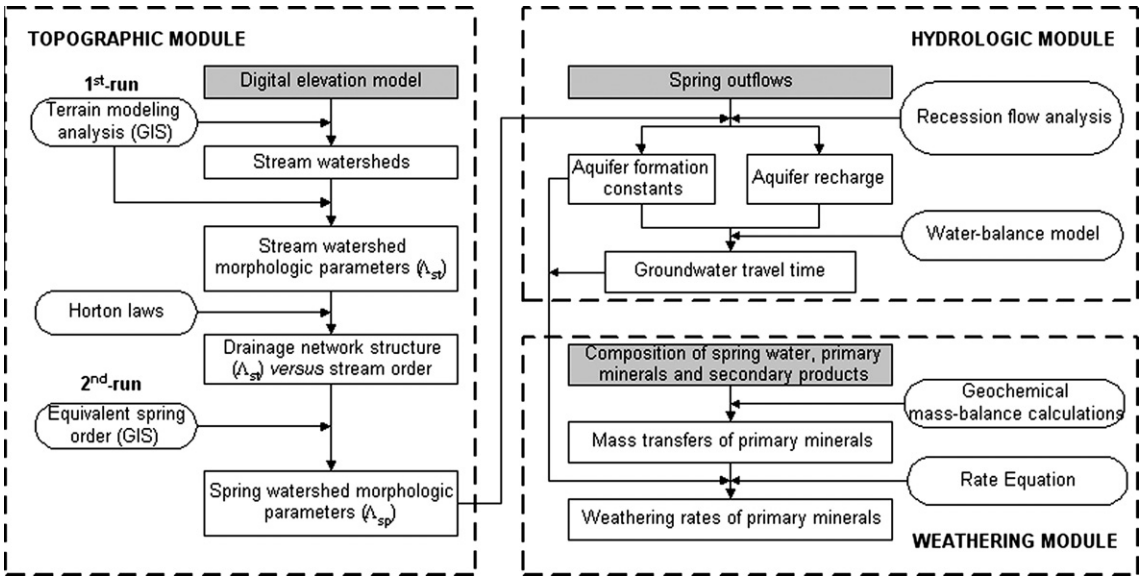

Fig. 3. Flowchart of the THROW model.

logic parameter (area or slope of the watershed, number or length of streams within the watershed) measured at order i and order $i+1$ is constant. According to Rosso et al. (1991), the Horton laws of network composition are geometric-scaling relationships because they hold regardless of the order or resolution at which the network is viewed and because they yield self-similarity of the catchment–stream system, or at least self-affinity in cases where the scaling factors in the longitudinal and transverse directions are not equal (Nikora and Sapozhnikov, 1993) or self-organization in cases where complex drainage networks are to be described as multi-fractal systems (De Bartolo et al., 2000, 2004, 2006; Gaudio et al., 2006). Because these laws typically hold for a wide range of scales in nature, they can be employed to extrapolate watershed morphologic parameters across scales. A generalized equation for the relationship between morphologic parameter Λ and order i can be written as:

$$\Lambda = f(i) \tag{1}$$

where f is a scaling function. Because springs usually emerge in the vicinity but away from the water channels their watersheds cannot be associated to a particular Strahler order. In general, neighboring channels differ from each other in their order and therefore watersheds of springs must be classified according to the concept of equivalent order (i_{eq}), which is defined here as an average of the orders of the surrounding streams. Unlike stream orders, which are integers, equivalent spring orders will be real numbers. When a spring site is situated in a region where, for example, $i_{eq} = 1.5$, this means that the catchment area of the spring is larger than the average area of 1st-order watersheds and smaller than the average area of 2nd-order watersheds. For spring watersheds, morphologic parameters are determined by Eq. (1), where i is replaced by i_{eq}.

4.1.2. Carrying out the topographic module on a GIS platform

The topographic module of the THROW model is executed on a Geographic Information System (GIS) comprising the ArcGIS (ESRI, 2007) and ArcHydro (ESRI, 2009) computer packages, and operates in two sequential runs (Fig. 3). In the first run, ArcHydro executes a terrain modeling analysis based on the Digital Elevation Model of the study area (e.g. Fig. 1), whereby the drainage network and watersheds are drawn and classified according to their Strahler orders. Subsequently, the same package assesses morphologic parameters of each watershed, including area, volume and length of water channels, and calculates average values for each order. Based on these average values, relationships between the parameters and concomitant orders (Eq. (1)) are defined using least squares regression. In the second run, the *Density Function* of ArcGIS toolbox is used to calculate equivalent orders for the spring watersheds. Firstly, the map with the drainage network is overlapped by a grid of cells with dimensions 100×100 m and, within each cell, the lengths of streams are measured (L_i) and multiplied by the corresponding order (i). Secondly, the previous step is repeated for every order appearing in the cell and then the products $L_i \times i$ are summed and divided by the total length of streams within the cell (L), giving the i_{eq}:

$$i_{eq} = \frac{\sum_{i=1}^{n} L_i \times i}{L} \tag{2}$$

The i_{eq} of a given spring watershed is determined from the map of equivalent orders computed using Eq. (2) by evaluating the i_{eq} at the location coordinates of the spring site. The corresponding morphologic parameters will be assessed afterwards using the i_{eq} values in Eq. (1).

4.2. The hydrologic module

This module aims on estimating hydrologic parameters of the fractured aquifer at the watershed scale. It comprises a set of methods to calculate hydraulic conductivity and effective porosity, evaluate annual recharge, and assess groundwater travel time. The module's flowchart is illustrated in Fig. 3. The data required for its operation encompass the outflows measured at the spring sites and results from the topographic module.

4.2.1. Spring outflows and aquifer hydraulic parameters

The outflow or discharge of a fracture artesian spring some time after a precipitation event occurs from upstream aquifers along the underground flow path to the spring. This type of flow is known as base flow and the analysis of base flows recognized as recession flow analysis. When combined with physically based flow equations, recession analysis can be used as a tool for aquifer characterization, namely for assessment of hydraulic conductivity and effective porosity (Szilagyi and Parlange, 1999; Szilagyi et al., 1998; Mendoza et al., 2003; Van de Giesen et al., 2005; Malvicini et al., 2005; among others).

For the analysis of spring outflows, the THROW model adopted a technique developed by Brutsaert and Nieber (1977) for stream flow

recession analysis, called the Brutsaert method. Declining groundwater reservoirs control both stream base flow recession and upland spring outflow recession, so the method should be equally valid for both situations. The use of the Brutsaert method is advantageous because it is independent of the ambiguity inherent in identifying when base flow starts (Malvicini et al., 2005). Refinements and extensions on the method have been made in Zecharias and Brutsaert (1985, 1998), Brutsaert (1994), Brutsaert and Lopez (1998), Rupp and Selker (2005); among others. The Brutsaert method is founded on the Boussinesq equation (Boussinesq, 1903, 1904), which describes the drainage from an ideal unconfined rectangular aquifer bounded below by a horizontal impermeable layer and flowing laterally into a water channel. There are several theoretical solutions of the Boussinesq equation that have the general form of a power function (Rupp and Selker, 2006):

$$\frac{dQ}{dt} = aQ^b \tag{3}$$

where Q ($m^3\ s^{-1}$) is the recession flow, t is time, and a and b are constants. The coefficient a can be directly related to the groundwater reservoir's characteristics and b is an exponent whose value depends on the recession flow regime. There are two distinct flow regimes: the short-time and the long-time regime. Short-time flows generally have a higher Q than long-time flows. Brutsaert and Lopez (1998) showed the following solution for short-time flow:

$$a = \frac{1.13}{Kn_eD^3L^3}, \quad b = 3 \tag{4a}$$

where K is the hydraulic conductivity, n_e the effective porosity, D the aquifer thickness and L the length of upstream channels intercepting groundwater flow. The long-time flow is adequately described by the so-called linear solution of Boussinesq (1903).

$$a = \frac{0.35\pi^2 KDL^2}{n_eA^2}, \quad b = 1 \tag{4b}$$

where A is the upland drainage area. Eqs. (4a) and (4b) can be combined to describe K and n_e as a function of a and the morphologic parameters of the watershed (A, D, L). On the other hand, D can be approached to the ratio V/A. In that case,

$$K = 0.57\sqrt{\frac{a_1}{a_3}}\left(\frac{A^3}{V^2L^2}\right) \tag{5a}$$

$$n_e = \frac{1.98}{V\sqrt{a_1a_3}} \tag{5b}$$

where a_i represents the value of a when $b = i$ (1 or 3).

To estimate K and n_e using Eqs. (5a) and (5b) it is required a previous run of the topographic module, the results of which provide numbers for A, V and L. The values of a_1 and a_3 can be read in a scatter plot of $\ln(\Delta Q/\Delta t)$ *versus* $\ln(Q)$. According to the Brutsaert method, the lower envelope of the scatter points is represented by two straight lines, one with a slope $b = 1$, and the other with a slope $b = 3$, and the y-values where the lines intercept $\ln(Q) = 0$ (or $Q = 1$) are the parameters a_1 and a_3.

4.2.2. Spring base flows and aquifer recharge

Recession flow analysis is also used as a tool for aquifer recharge estimation. In this case, recession segments are selected from the hydrographic record of the spring and their geometric properties (e.g. slope) combined with analytical models to provide measures of the aquifer recharge. Underlying the methods of recession flow analysis is the storage-outflow model adopted to represent discharge from natural storage compartments during the recession phase. Many complex functions have been developed in this context, for example to explain the outflow from karstic aquifers (Padilla et al., 1994), channel banks (Cooper and Rorabaugh, 1963), surface depressions such as lakes or wetlands (Griffiths and Clausen, 1997), etc., but many other recession flow models assume a linear relationship between storage and outflow, described by the classic exponential decay function of Boussinesq (1877):

$$Q = Q_i e^{-\alpha t} \tag{6}$$

where Q_i is the base flow at the beginning of a recession period and α is the recession constant. One of these methods has been developed by Meyboom (1961) and is now incorporated into the THROW model. Starting with Eq. (6), Meyboom (1961) noted that a plot of discharge *versus* time on a semilogarithmic paper would yield a straight line, the slope of which defines the recession constant. In this case, the Eq. (6) can be re-written as:

$$Q = \frac{Q_i}{10^{t/t_1}} \tag{7}$$

where t_1 is the time corresponding to a log-cycle of discharge. Integrating Eq. (7) from $t = 0$ (beginning of the recession) and $t =$ infinity (complete depletion of the aquifer) gives:

$$V_t = \frac{Q_i t_1}{2.3} \tag{8a}$$

where V_t is the total potential groundwater discharge. By analogy, the residual potential groundwater discharge (V_s) can be approached by:

$$V_s = \frac{Q_f t_1}{2.3} \tag{8b}$$

where Q_f is the base flow at the end of the recession phase. Considering a sequence of two recession periods, aquifer recharge (V_r) between periods will be defined as the difference between V_t, evaluated at the beginning of period 2, and V_s estimated at the end of period 1, i.e.:

$$V_r = (Q_i - Q_f)\frac{t_1}{2.3} \tag{9}$$

4.2.3. Groundwater travel times

Groundwater transit (or travel) time is defined as the elapsed time when the water molecules exit the flow system (Bolin and Rodhe, 1973; Etcheverry and Perrochet, 2000; Rueda et al., 2006). A point of reference for mean transit times are often the hydraulic turnover times, since they define the turnover timescale based on the best understanding or assumption of the catchment subsurface volume and mobile storage if the unsaturated zone transit time is small compared to the total transit time of the system. The concept of hydraulic turnover time was adopted by the THROW model to estimate the travel time of groundwater within the spring watershed boundaries (t, s). According to McGuire and McDonnell (2006), if a simple water balance is considered, the hydraulic turnover time is defined as the ratio of the mobile catchment storage (equated to Vn_e, m^3) to the volumetric flow rate (equated to the aquifer recharge: V_r, $m^3\ s^{-1}$):

$$t = \frac{Vn_e}{V_r} \tag{10}$$

4.3. Weathering module

This module combines the chemical composition of spring waters and of their host rocks in a mass balance algorithm to calculate the number of moles of primary minerals and of secondary products dissolved or precipitated along the flow path. In a subsequent stage, these mass transfers are combined with aquifer hydraulic parameters and groundwater travel time in a rate equation to obtain mineral weathering rates (Fig. 3).

4.3.1. Geochemical mass balance calculations

There are essentially two types of geochemical models for assessing mineral weathering rates at the watershed scale. The first

approach estimates solid-state weathering rates based on the differences between elemental, isotopic and mineral compositions measured in present-day regoliths and in the assumed protolith. In this case, rates represent the entire time span of a weathering episode, commonly on the order of thousands to million years. The second approach calculates solute-flux rates that stand for contemporary weathering during groundwater percolation in the rocks, in which case time is a window to the weathering episode spanning few years or decades. The THROW model is based on the solute-flux approach and uses the SiB algorithm of Pacheco and Van der Weijden (1996), extended by Pacheco et al. (1999) and Pacheco and Van der Weijden (2002), to perform the geochemical mass balance calculations. A brief description of the method is given in the next paragraphs.

The SiB algorithm comprehends a set of mole balance and charge balance equations of the form:

$$\text{Mole balance equations} - \sum_{j=1}^{q_1} \beta_{ij}[\mathrm{M}_j] + [\mathrm{Y}_i]_\mathrm{p} = [\mathrm{Y}_i]_\mathrm{t}, \text{ with } i = 1, q_2 \quad (11a)$$

$$\text{Charge balance equation} - \sum_{l=1}^{q_3} z_l[\mathrm{Y}_i]_\mathrm{p} = [\mathrm{Cl}^-]_\mathrm{t} + 2[\mathrm{SO}_4^{2-}]_\mathrm{t} + [\mathrm{NO}_3^-]_\mathrm{t} \quad (11b)$$

where q_1, q_2 and q_3 are the number of primary minerals involved in the weathering process, the number of inorganic compounds that usually are released from weathering reactions ($q_2 = 6 = \mathrm{Na}^+$, K^+, Mg^{2+}, Ca^{2+}, HCO_3^- and $\mathrm{H_4SiO_4^0}$), and the number of the latter compounds that usually are also derived from atmospheric plus anthropogenic sources – lumped as "pollution" ($q_3 = 4$ = the four major cations); suffixes t and p mean total and derived from "pollution", respectively. The expected sources of anthropogenic pollution are manures, commercial fertilizers and domestic and(or) industrial effluents; Y represents a dissolved compound; M represents a mineral; Cl^-, SO_4^{2-} and NO_3^- are the major dissolved anions assumed to represent exclusively atmospheric plus anthropogenic inputs; square brackets ([]) denote concentrations of a dissolved compound or a dissolved mineral; b_{ij} is the ratio of the stoichiometric coefficients of dissolved compound i and mineral j, as retrieved from the weathering reaction of mineral j; $b_{ij}[M_j] = [Y_i]r_j$, where $[Y_i]r_j$ is the concentration of a dissolved compound i derived from reaction of M_j moles of mineral j; z_l is the charge of cation l.

The number of equations in Set 11a,b is seven. The unknowns of the system are the $[M]$ and the $[Y]p$ variables, in total $q_1 + q_3$. The SiB algorithm uses the Singular Value Decomposition procedure as described in Press et al. (1991) to solve the set of equations because this procedure can handle efficiently (through least squares or minimizing procedures) the cases where the set is undetermined ($q_1 + q_3 > 7$) or overdetermined ($q_1 + q_3 < 7$). In systems with fluid flow, precipitation of secondary products along the flow path follows certain sequences (Helgeson et al., 1969; Steefel and Lasaga, 1992; Steefel and Van Cappellen, 1990). The SiB algorithm describes these sequences as reactions of primary minerals to mixtures of secondary products (for example alteration of plagioclase to $c_1 \times$ halloysite + $(1 - c_1) \times$ gibbsite, with $0 \leqslant c_1 \leqslant 100\%$; alteration of biotite to $c_2 \times$ vermiculite + $(1 - c_2) \times$ halloysite, with $0 \leqslant c_2 \leqslant 100\%$). Only a few of these mixtures will explain the chemical composition of the spring waters. To be labeled as valid mixture, the selected values of c_1 and c_2 must result in a solution of Set (11a) and (11b) satisfying $[M] \geqslant 0$ and $[Y]p \geqslant 0$. Among the valid mixtures, the SiB algorithm selects a best-fit one by checking all against predefined external boundary conditions.

4.3.2. Rate equation

The weathering rate of a mineral M is commonly defined by the relationship:

$$W_M = \frac{[M]}{t} \times \frac{V_r}{A_M} \quad (12)$$

where W_M (mol m^{-2} s^{-1}) is the rate and $[M]$ (mol m^{-3}) its concomitant dissolved concentration, t (s) is the average travel time of water packets flowing through the spring watershed, V_r (m^3) is the volume of water entering the spring watershed in a unit time, and A_M (m^2) is the surface area of M in contact with that volume of aquifer water. To adequately describe the reactive surface area of a fracture artesian spring watershed, weathering modules must incorporate rock structure in the calculation of A_M. This is accomplished by the THROW model. In this model, A_M is calculated by a formula developed by Pacheco and Alencoão (2006) describing the area of fracture surfaces in contact with aquifer water in unit time:

$$A_M = 2\alpha_M V_r \times \sqrt{\frac{\rho_w g n_e}{12\mu_w K}} \quad (13)$$

where α_M is the proportion of mineral M in the rock, μ_w is the dynamic viscosity of water (1.14×10^3 kg s^{-1} m^{-1} at $T = 15$ °C), and g is the acceleration of gravity (9.81 m s^{-2}). Replacing this equation in Eq. (12) and rearranging gives:

$$W_\mathrm{M} = \frac{[\mathrm{M}]}{2t\alpha_\mathrm{M}} \sqrt{\frac{12\mu_w K}{\rho_w g n_e}} \quad (14)$$

Derivation of Eq. (14) stands on four fundamental assumptions. The first assumption is that water in a thin soil cover percolates mainly through the macropores (Hornberger et al., 1990; Velbel, 1993; Drever, 1997; Rodhe and Killingtveit, 1997), resulting in relatively short transit times to the fracture network lying beneath, where water–mineral interactions will take place. The second assumption is that flow in fractured rock units is limited to preferential flow paths and is slow given the typically low hydraulic conductivity, thus resulting in extended travel time. The third assumption is that infiltrating water pushes the old water ahead according to piston flow (Appelo and Postma, 2005), meaning that solute transport occurs predominantly by advection. Eq. (14) does not account for the time required by solutes to travel from dead ends along microfractures to gravity flow fractures by diffusion (Meunier et al., 2007). Weathering rates calculated by this equation may thus be overestimated. The fourth assumption is that the area available for weathering reactions is restricted to minerals facing fracture walls with the same composition as the rocks in which they occur, although this assumption is not valid for fractures that have been lined with silica or other secondary products. Under such circumstances, the spring water chemistry will be dominated by water–mineral interactions along the dominant flow paths and, more importantly, by contact with the fracture walls and not by interactions with the whole inventory of minerals and soils and solid rocks in the aquifer.

5. Results

5.1. Results of the topographic module

The topographic module of the THROW model (Fig. 3) was applied to the Digital Elevation Model of Vouga basin (Fig. 1), in the sector where springs were sampled (the granite area; Fig. 2). Firstly, ArcHydro (ESRI, 2007) was used to delineate watersheds within that area, taking into account the order i of the associated stream. The results are illustrated in Fig. 4a. The number of 1st-order watersheds is 1241, covering an average area $A = 0.44$ km^2 watershed^{-1}, whereas the whole granite area encompasses a 6th-order watershed with an area $A = 955.39$ km^2. A plot of A *versus* i (Fig. 4b) shows a firm correlation between these variables, confirming that Horton laws of network composition hold for the studied area. In keeping with this

observation, the generalized relationship between morphologic parameters and order (Eq. (1)) can, for the granite area of the Vouga River basin, be replaced by the function fitting the scatter points in Fig. 4b. Using a least squares method, it was found that such function is represented by an exponential equation:

$$A = 0.1e^{1.49\times i} \quad (R^2 = 0.99) \tag{15}$$

Secondly, a map of equivalent orders (i_{eq}) was drawn for the granite area (Fig. 5) and discrete orders were determined for each spring by evaluating the i_{eq} at the location coordinates of the spring site. The results are summarized in Appendix A. Most sampled springs (94%) emerge where i_{eq} = 1–3. Eq. (15) can be used to extrapolate the catchment area of the springs if i is replaced by i_{eq} in this equation. These areas vary from 0.4 to 180.9 km^2, although most of them (the ones with i_{eq} = 1–3) are smaller than 10 km^2. These results, also summarized in Appendix A, are consistent with previous reports (Pacheco and Van der Weijden, 2002).

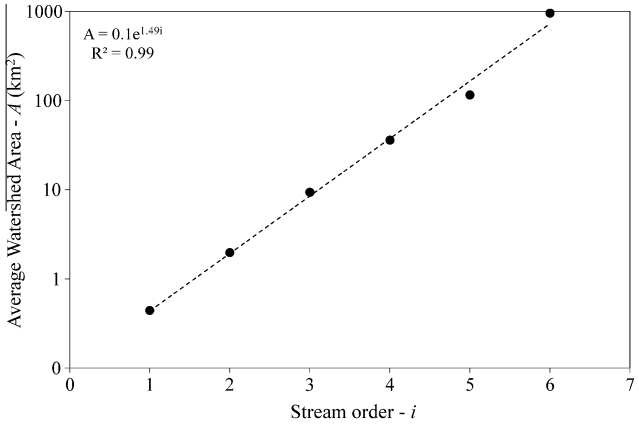

Fig. 4b. Plot of stream watershed area as a function of Strahler order, illustrating the firm relationship existing between these variables.

5.2. Results of the hydrologic module

5.2.1. Aquifer hydraulic parameters and travel times of stream watersheds

The hydrologic module of the THROW model (Fig. 3) could not be applied to the studied springs because the required spring outflows were lacking. To compensate for this, the hydrologic characterization of the region was based on the application of the THROW model to seven stream watersheds located upstream of the hydrometric stations represented in Fig. 1. The hydraulic conductivities (K) and effective porosities (n_e) resulting from this characterization were then used as proxies of the K and n_e values of the spring watersheds, as explained in the next section, which also describes how groundwater travel times were downscaled from the larger (stream) the smaller (spring) scales.

The hydrologic characterization of the stream watershed is summarized in Table 1. The initial stage of topographic characterization (1st-run of the topographic module; Fig. 3) indicated that watershed areas (A) range from 22 to 649 km^2, watershed volumes (V) from 7 to 317 km^3 and water channel lengths (L) from 24 to 177 km. Subsequent application of the Brutsaert method gave numbers for hydraulic conductivity (K) and effective porosity (n_e). The application of the method to Station 1 (location given in Fig. 1) is illustrated in Fig. 6. In this figure, black dots represent 17 years of monthly average stream

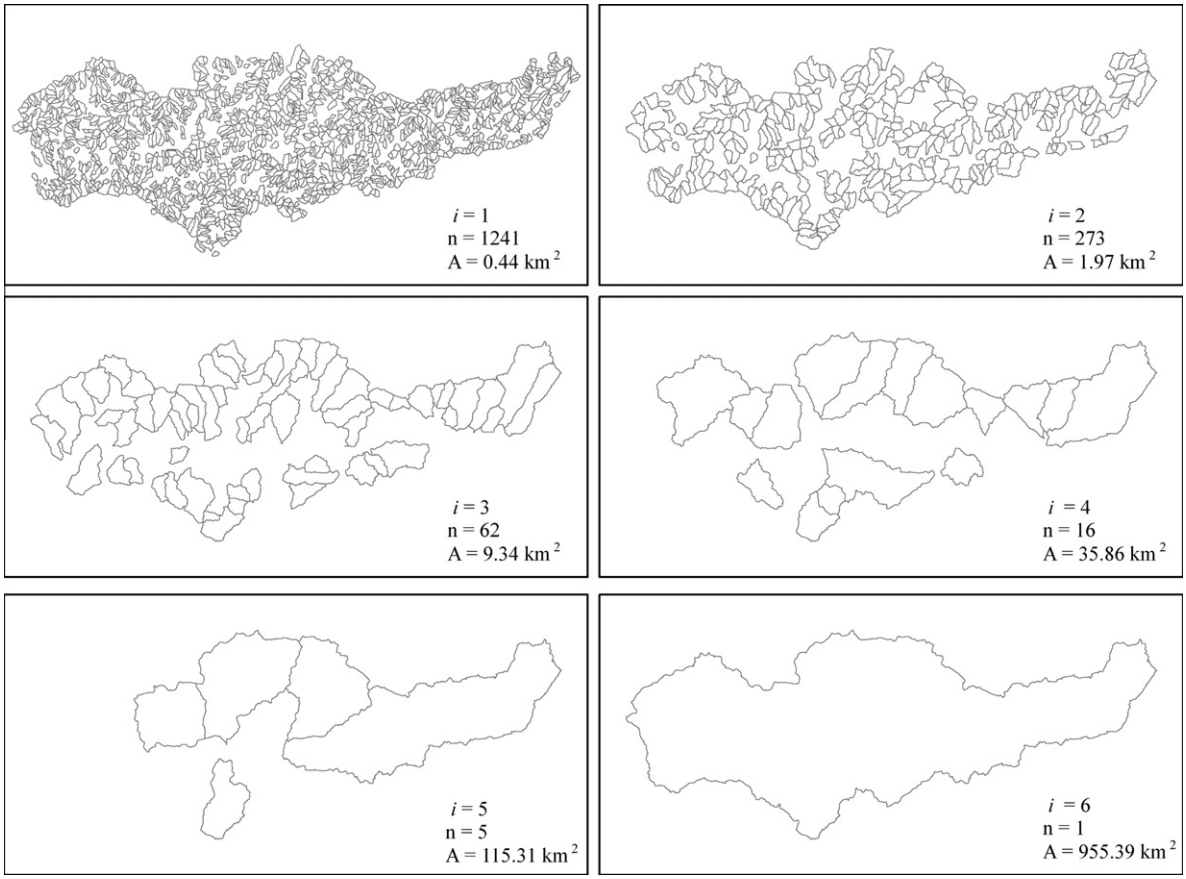

Fig. 4a. Distribution of watersheds within the granite area of the Vouga basin, taking into account their order of Strahler (classification according to Strahler, 1957). Symbols: i – Strahler order; n, A – number and average area of watersheds of a given order.

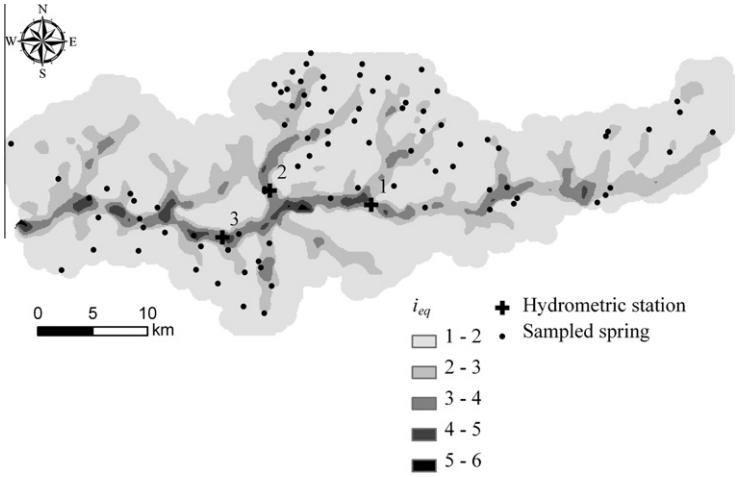

Fig. 5. Distribution of equivalent spring orders (shaded areas) and location of the sampled (circles), within the granite area of the Vouga basin. Location of hydrometric stations labeled Id = 1–3 in Table 1. Symbol: i_{eq} – equivalent spring order (calculated by Eq. (2)). The i_{eq} under each spring can be used in Eq. (15) (replacing i) to extrapolate the area of its associated watershed.

flows compiled from the hydrographic record of the station (period 1936/37–1953/54), available at the Portuguese National Water Institute (www.inag.pt). The dashed lines are the lower envelopes to the scatter points. According to the Brutsaert method, the intercept-y of these lines are parameters a_1 and a_3 of Eqs. (5a) and (5b). For Station 1, $\log(a_1) = -19.5$ and $\log(a_3) = -22.5$. Combining these values with morphologic parameters of the watershed (A, V, L; Table 1) in Eqs. (5a) and (5b) gives $K = 2.4 \times 10^{-7}$ m s^{-1} and $n_e = 3.7 \times 10^{-2}$. The average K and n_e, when considering the values obtained for the seven watersheds, are $(4.7 \pm 3.2) \times 10^{-7}$ m s^{-1} and $(2.0 \pm 1.3) \times 10^{-2}$, respectively. These values are consistent with fractured rock hydraulic conductivities and effective porosities (Domenico and Schwartz, 1990). Application of the hydrograph method of Meyboom (1961) provided estimates for the aquifer recharge (V_r). The application of the method to Station 1is illustrated in Fig. 7. As in Fig. 6, the black dots are discharge rate measurements representative of a given month. The straight lines are fits to base flows of the recession periods. They are parallel because their slope is a function of the aquifer hydraulic parameters (K and n_e), which do not change over the time scales represented in the graph (2 years). Based on the geometry of the dashed lines and on its relation with the base flow measurements, values were determined for Q_f (180 L s^{-1}), Q_i (21,000 L s^{-1}) and t_1 (100 days), which have been used in Eq. (9) to calculate V_r (78×10^6 m^3). This value is valid solely for the hydrologic years 1939/40 and 1940/41, represented in Fig. 7. For the entire record length of Station 1 (17 hydrologic years), the average aquifer recharge is 57×10^6 m^3, and when the seven stations are taken altogether, $V_r = (53 \pm 39) \times 10^6$ m^3 (Table 1). Finally, using the values of V, n_e and V_r in Eq. (10), average travel times of groundwater in the seven stream watersheds were calculated, varying from 7 to 107 years (Table 1).

5.2.2. Aquifer hydraulic parameters and travel times of spring watersheds

The hydrologic parameters of spring watersheds were extrapolated from the values assessed at larger scales (previous section). Fig. 8 plots travel time, hydraulic conductivity and effective porosity as a function of watershed area, using the values calculated for the seven stream watersheds (Table 1). The relationship between the hydrologic parameters and area is unequivocal, being expressive for t as:

$$t = 0.16A + 1.37 \quad (R^2 = 0.98) \qquad (16)$$

The higher K and n_e values of larger basins reflect the accentuated heterogeneity of these basins relative to the smaller ones (Domenico and Schwartz, 1990). The longer travel times are inherently associated to longer flow paths. According to Eq. (14), a simultaneous increase in K and n_e has a limited impact on the estimates of weathering rates (W), because W is a function of $\left(\sqrt{K/n_e}\right)$. For the seven watersheds, the minimum value of $\sqrt{K/n_e}$ is 2.5×10^{-3} m$^{1/2}$ s$^{-1/2}$, whereas the maximum is 8.2×10^{-3} m$^{1/2}$ s$^{-1/2}$, so, regardless the values adopted for the aquifer hydraulic parameters the impact on weathering rates would not exceed a factor of 3.2. Contrarily to K and n_e, changes in t have a tremendous impact on those estimates, because W is a function of $1/t$. Based on this assessment, it was assumed that K and n_e were constant within the catchment areas of the springs and equal to the mean values estimated for the seven stream watersheds (Table 1): $K = 4.7 \times 10^{-7}$ m s^{-1} and $n_e = 2.0 \times 10^{-2}$. On the other hand, Eq. (16) was used to extrapolate (downscale) travel times for spring waters. These times varied from 1.4 to 30.3 years, but for springs with $A < 10$ km^2, they ranged from 1.4 to 2.8 years. The entire record of spring water travel times is depicted in Appendix A.

5.3. Results of the weathering module

The hydrochemistry of springs in the Vouga basin and the chemical weathering of associated granites and metassediments have been discussed in great detail by Van der Weijden and Pacheco (2006). This study encompassed an application of the SiB algorithm to the spring water compositions summarized in Appendix A. The SiB mole balance calculator is one of the THROW model components. For that reason, the results obtained in 2006 were adopted for the present study, being summarized in Appendix B. In brief, the analytical data indicated that chemical weathering of plagioclase and biotite determined the inorganic chemical composition of the springs. For plagioclase, it was calculated an average mass transfer of [Pl] = 148 ± 56 micromoles per liter of water. In the geochemical calculations, it was assumed that plagioclase weathered into mixtures of halloysite and, depending on whether rainfall was larger or smaller than 1000 mm y^{-1}, gibbsite or smectite. It was also assumed that weathering of biotite produced mixtures of halloysite and vermiculite. The results showed that weathering of plagioclase produced [smectite] = 2 ± 11 μM, [halloysite] = 68 ± 42 μM and [gibbsite] = 14 ± 21 μM, i.e. that halloysite is the dominant secondary product precipitating along the flow paths.

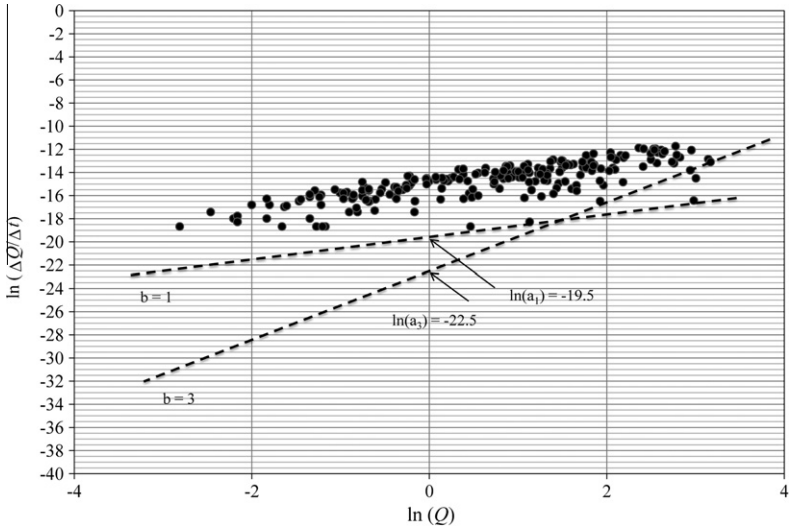

Fig. 6. Application of the Brutsaert method to the watershed located upstream Station 1 (see location in Fig. 1). The original data used in the plot pertains to the 1936–53 period and is available at www.inag.pt. The method is used to calculate the average watershed hydraulic conductivity and effective porosity (Eqs. (5a) and (5b)): $K = 2.4 \times 10^{-7}$ m s^{-1}; $n_e = 3.7 \times 10^{-2}$.

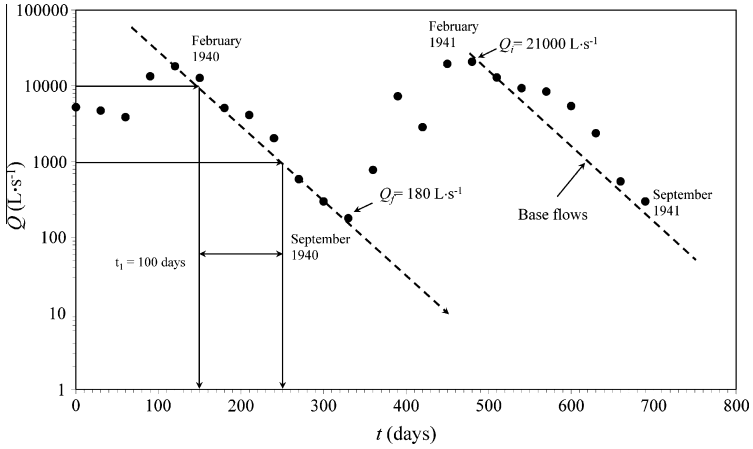

Fig. 7. Stream hydrograph of Station 1 (see location in Fig. 1 and summary of data in Table 1). The record of discharge rate measurements (Q) is available at www.inag.pt. Illustration of the hydrograph method used for the estimation of V_r (Meyboom, 1961), taking into account the values of Q_i, Q_f, and t_1 obtained for the 1939/40 and 1940/41recessions. The explanation of the symbols is given in the text. For this pair of recession periods, $V_r = 78 \times 10^6$ m^3 (Eq. (9)).

For the calculation of plagioclase weathering rates (W_{Pl}), it was assumed that the weight fraction of this mineral in the granites was consistently $\alpha_{PL} = 0.31$. The remaining input data to the rate equation (Eq. (14)) are the dissolved concentrations of plagioclase ([Pl]) reported in Appendix B, the spring water travel times of (t) listed in Appendix A, and the aquifer hydraulic parameters ($K = 4.7 \times 10^{-7}$ m s^{-1} and $n_e = 2.0 \times 10^{-2}$). The calculated W_{Pl} values are within the interval $(2.5 \pm 1.2) \times 10^{-14}$ mol m^{-2} s^{-1} ($-\log(W) = 13.7 \pm 0.3$).

6. Discussion

6.1. Thermodynamic validation of the SiB results

The concentrations of dissolved plagioclase ([Pl]) and the amounts of precipitated secondary products ([gibbsite], [halloysite] and [smectite]) were determined by Van der Weijden and Pacheco (2006) using mole balance calculations and are listed in Appendix B. These results are supported by equilibrium models. Paces (1978) reviewed the secondary phases that may control the concentrations of Al and Si in natural waters. The order of increasing stability of aluminum hydroxide phases is amorphous $Al(OH)_3$, microcrystalline gibbsite, and gibbsite. The same order for aluminosilicates is allophane, halloysite, and kaolinite. The calculated Q/K_{eq} ratios of these secondary phases, where Q is the ion activity product (IAP) calculated from the activities of the relevant dissolved species (Appendix A) and K_{eq} is the solubility product, are reported in Appendix B (Columns 8–13). Plots of the actual total Al concentrations in the spring waters against pH (Appendix A) can be compared with the equilibrium curves of these phases (Fig. 9a and b). The distribution of the measured values as well as the Q/K_{eq} values given in Appendix B show that springs were in close equilibrium with microcrystalline gibbsite and halloysite/allophane. Precipitation of metastable phases along the flow path of the fluids is consistent with the Ostwald Step Rule. In general, Al hydroxide phases are expected to precipitate first, followed by precipitation of aluminosilicates (Helgeson et al., 1969; Steefel and Lasaga, 1992). The studied spring waters represented a mixture of water packets that followed different flow paths with different velocities. Because the flow of groundwater across the granites is essentially through fissures and fractures, it is impossible to determine exactly where the secondary products precipitate. Simultaneous equilibrium with respect to gibbsite and halloysite,

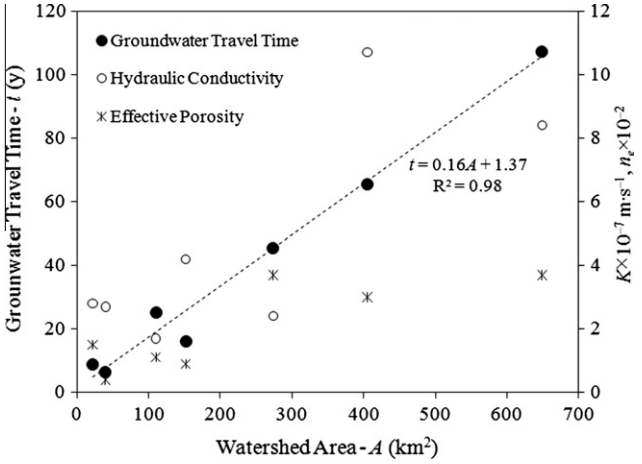

Fig. 8. Plot of hydraulic conductivity, effective porosity and groundwater travel time, as a function of stream watershed area, illustrating the unequivocal (firm in the case of t) relationship existing between these variables.

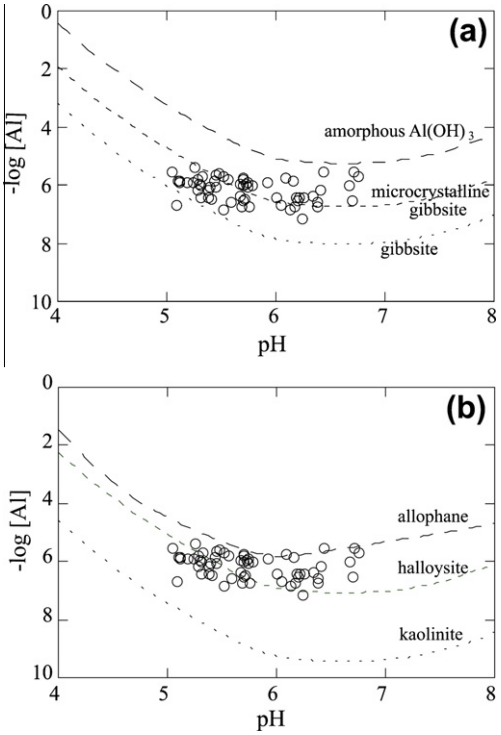

Fig. 9. Total Al concentrations (open symbols), as far as they were determined, and theoretical total concentrations (curves) plotted against pH for (a) crystalline gibbsite, microcrystalline gibbsite and amorphous $Al(OH)_{3(s)}$, and (b) kaolinite, halloysite and allophane. Total Al concentrations and pH values at the sampling sites are listed in Appendix A. The curves for the solid phases as a function of pH are calculated from data in Nordstrom et al. (1990) for $Al(OH)_3$-phases and in Langmuir (1997) for the Al-silicate phases. In the last case, the $H_4SiO_4^0$ activity was fixed at its median value (Appendix A). Note that the distances between the curves for each solid phase turn out to be only very small when instead of the median value the minimum and maximum values of $H_4SiO_4^0$ activities would have been used. It appears that the solutions are most closely in equilibrium with microcrystalline gibbsite and(or) halloysite/allophane (cf. also Columns 8–13 in Appendix B).

as calculated for 34 spring waters, could have occurred in a wider or narrower band along a characteristic flow path, depending on the hydrodynamic dispersion (Steefel and Lasaga, 1992). Moreover, the ratio between the kinetic dissolution and precipitation constants of the primary and secondary phases may have stretched the apparent stability fields of these phases, resulting in overlap instead of separation (Steefel and Van Cappellen, 1990). The generally strong relation between the presence of 'gibbsite' (SiB results) and degree of saturation with respect to microcrystalline gibbsite is shown in Fig. 10. The calculated amount of gibbsite precipitates ([Gibbsite] > 0) generally occurred within a rather narrow band of low saturation values. The samples with high Q/K_{eq} values relative to microcrystalline gibbsite were closer to equilibrium with amorphous $Al(OH)_3$ (Appendix B). Analytical uncertainties in the determination of total dissolved Al, and consequently in the $\{Al^{3+}\}$ values, were propagated in the accuracy and precision of the calculated Q values. For this reason, no rigid meaning is attributed to Q/K_{eq} values smaller than 1. The general correspondence between the results of the mass balance method (SiB) and the concomitant calculated equilibria makes a strong case for the precipitation of the metastable phases.

6.2. Residual undersaturation of spring waters with respect to plagioclase

The congruent dissolution of plagioclase can be represented by the reaction:

$$Na_{1-x}Ca_xAl_{1+x}Si_{3-x}O_8 + 4(1+x)H^+ + 4(1-x)H_2O \rightarrow (1-x)Na^+ + xCa^{2+} + (1+x)Al^{3+} + (3-x)H_4SiO_4^0 \quad (R1)$$

with $K_{eq} = \{Na^+\}^{(1-x)}\{Ca^{2+}\}^x\{Al^{3+}\}^{(1+x)}\{H_4SiO_4^0\}^{(3-x)}/\{H^+\}^{4(1-x)}$

where x is the mole fraction of anorthite in plagioclase and {} represents activity.

The actual ion activity product (IAP) for reaction (R1), calculated on the basis of the analytical data (Appendix A), is generally smaller than K_{eq}. As explained in Appendix B, the degree of undersaturation can be expressed as the Gibbs free energy of dissolution (ΔG_r). Most springs are undersaturated with respect to plagioclase (negative ΔG_r), the exceptions being springs 2070, 2071 and 2072 (Appendix B, last column). ΔG_r has been used as a key parameter in many kinetic dissolution models (Beig and Lüttge, 2006; Lasaga, 1998; Lüttge, 2006; Maher et al., 2009; and numerous references therein). Its role in such models becomes more important as the solution approaches equilibrium ($\Delta G_r \rightarrow 0$). Dissolution rates are highest and constant far from equilibrium (i.e., the so-called dissolution plateau). During ongoing dissolution, undersaturation decreases and approaches equilibrium in a linear fashion or in a sigmoidal manner characterized by a typical critical ΔG_r^{crit}, beyond which the dissolution mechanism dramatically changes from a rapid to a slow mode, proceeding linearly until equilibrium is realized (Burch et al., 1993; Hellmann and Tisserand, 2006). Other modes of dissolution rates as a function of ΔG_r have been observed and can be explained by the presence and persistence of etch pits on the dissolving mineral surface (Oelkers et al., 1994; Lüttge, 2006). Further discussion of the processes and mechanisms, and the underlying theories and observations is beyond the scope of this paper. It is worth mentioning, however, that the median and average values of ΔG_r (–20 kJ mol^{-1}), as well as that of almost all individual values calculated for the spring waters, were higher than the ΔG_r^{crit} of about –28 ± 3 kJ mol^{-1} for albite (Burch et al., 1993; Arvidson and Lüttge, 2010), and were at least close to $\Delta G_r^{crit} \approx -18$ kJ mol^{-1} (Lasaga and Lüttge, 2004; Lüttge, 2006). This means that the rate of plagioclase dissolution had already slowed once the ground water arrived at the spring site. It must be realized, however, that the rates must have been much higher when the ground waters started their journey along the flow channels. Considering that only the water composition at the terminals of the water flow were known, the data do not allow for comparisons of the calculated weathering rates with kinetic models of the dissolution rates of the plagioclases.

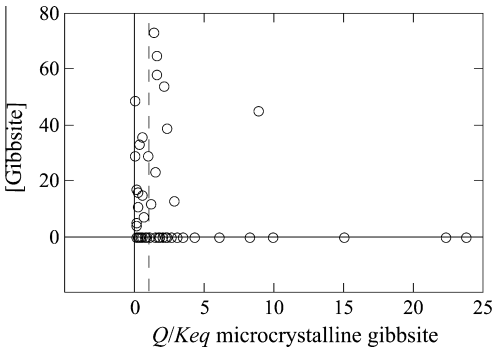

Fig. 10. Plot of the calculated amounts(*) of 'gibbsite' precipitated from the ground water as result of ongoing dissolution of plagioclase, against the calculated degree of saturation of microcrystalline gibbsite (Appendix B). Quite a few samples for which precipitation of 'gibbsite' was calculated (SiB results) are indeed close to equilibrium (cf. also Appendix B, Column 9) with microcrystalline gibbsite. For the other samples, no precipitation of 'gibbsite' was calculated, but many of these samples are also located in areas where $P < 1000$ mm year^{-1}, areas where the occurrence of gibbsite in soils is unlikely (Martins et al., 1995). Some waters (springs nrs. 1038, 2070, 2079, 2089 and 2101), although highly supersaturated relative to microcrystalline gibbsite ($Q/K_{eq} > 5$) and located in areas where $P > 1000$ mm year^{-1} (see Appendix B), had nonetheless [Gibbsite] = 0 μM. (*)We recognize that the presence, not the amount of 'gibbsite' matters.

Table 2
Summary of field weathering rates (W, mol m^{-2} s^{-1}) of oligoclases. References other than this study: (1) Drever and Clow (1995), (2) Velbel (1985), (3) White et al. (2001), (4) White and Brantley (2003).

–log(W)	Exposed surface estimation	Remarks	Reference
13.7 ± 0.3	Fracture	Average value (n = 87)	This study
12.7	Geometric	Average value (n = 2)	1
12.05	Geometric	Single value	2
12.9 ± 1	Geometric	Average value (n = 5)	3
15.0 ± 1.7	BET	Ditto (n = 3)	
12.7 ± 1.2	Geometric	Average value (n = 4)	4
14.7 ± 1.3	BET	Ditto (n = 15)	

6.3. Rates of plagioclase weathering

6.3.1. Comparison with reported weathering rates

Weathering rates calculated in the present study ($(2.5 \pm 1.2) \times 10^{-14}$ mol m^{-2} s^{-1}) are very close to the range of rates reported for Panola granite plagioclase: $(0.21 - 7) \times 10^{-14}$ mol m^{-2} s^{-1} (White and Brantley, 2003) measured in column-flow experiments after 6.2 years. Commonly reported laboratory rates are, on average, around 4×10^{-12} mol m^{-2} s^{-1} (White and Brantley, 2003), and are thus two to three orders of magnitude higher than the W_{Pl} determined by this study. Laboratory experiments, however, are usually conducted far from equilibrium conditions, with higher fluid/rock ratios than field conditions, and under high temperatures and low pH, which accelerate the dissolution reactions. Some experiments are conducted at ambient temperatures and at field-similar pH, but researchers rarely attempt to restrict the fluid/rock ratios or use pre-weathered samples.

The weathering rates reported in this study can also be compared with the field weathering rates reported by other studies (Table 2). Considering the differences in weathering conditions (climate, temperature, vegetation, soil thickness, age, etc.) and problems related to the determination of exposed surface areas, the range of reported values is not surprising. Arvidson and Lüttge (2010) argued that the complex chemical and thermal histories of the minerals along the reaction path have importance for mineral reactivity in natural basins. This may thus be the cause of the apparent variability in the reaction rates under natural weathering conditions. In addition, weathering rates correlate better with the fluid residence times than with the age of the weathering materials (Maher, 2010). The W_{Pl} values determined in our study depended on the calculated travel times of the fluids and surface areas exposed to the fluids. Given these uncertainties, the weathering rates for oligoclase obtained in our study compare well with the results obtained by other studies, as summarized in Table 2.

6.3.2. Influence of the exposed surface area

In the THROW model section (hydrologic module), a formula hinging on the volumetric fracture density concept was presented and used to estimate the exposed surface area (Eq. (13)). This method requires prior knowledge of the aquifer recharge (V_r), which is available for sub-basins of the Vouga basin (Table 1). The exposed surface areas calculated by this method for these sub-basins were $A_{Pl} = 4.79 \times 10^{11} - 1.19 \times 10^{13}$ m^2 (median 3.83×10^{12} m^2). If all plagioclase grains were in contact with the flowing groundwater, and not only the grains facing the fracture walls, then the exposed surface area would be given by:

$$A_{Pl} = \gamma_{Pl} S_{Pl} \tag{17}$$

where γ_{Pl} (kg) is the mass of plagioclase grains in contact with aquifer water in unit time (1 year) and S_{Pl} (m^2 kg^{-1}) is the geometric surface area of oligoclase, assumed to be 24.7 ± 14.0 m^2 kg^{-1} (Blum, 1994). The value of γ_{Pl} can be deduced from the annual recharge (V_r, m^3), the effective porosity of the aquifer, the weight fraction of plagioclase (α_{Pl}) in the rock, and the specific weight of plagioclase (ρ_{Pl}, kg m^{-3}), as follows:

$$\gamma_{Pl} = \frac{V_r}{n_e} \alpha_{Pl} \rho_{Pl} \tag{18}$$

Considering that the weight fraction of plagioclase in the Vouga granites is on average 0.31, and the specific weight of oligoclase is 2650 kg m^{-3}, the calculated area of oligoclase in the sub-basins, determined using Eq. (17), is $A_{Pl} = 1.67 \times 10^{13} - 1.03 \times 10^{14}$ m^2 (median 5.04×10^{13} m^2). The ratios between the exposed surface areas, estimated using Eqs. (13) and (17), are $1.34 \times 10^{-2} - 3.75 \times 10^{-1}$ (median 8.63×10^{-2}). The results show that, due to the inhomogeneous fluid migration through the fracture networks, the area of fluid–mineral interactions is reduced to some 9% of the total area available for reaction. Identical results were obtained by Pacheco and Alencoão (2006).

7. Conclusions

The THROW model, introduced in this paper, produced realistic estimates of morphologic and hydrologic parameters at the spring watershed scale, and of plagioclase weathering rates in granite environment. It is therefore appropriate to model mineral weathering in the vicinity of fracture artesian springs. The distinctive points of the THROW model include an assessment of morphologic parameters of spring watersheds based on scaling properties of the drainage networks, known as the Horton laws (Horton, 1945), and an evaluation of the area of minerals exposed to the percolating fluids using a formula based on fracture spacings, openings and porosities (Snow, 1968; Pacheco and Alencoão, 2006). The methods used to estimate spring watershed areas and groundwater travel times indicate that most fracture artesian springs in the Vouga basin granites are fed by catchments with areas ranging from 0.4 to 8.9 km^2, and that the travel time of water emitted from these springs is 1.4 to 2.8 years. The chemical composition of the springs, all sampled in the early summer season, is the result of weathering of minerals exposed to percolating waters at fracture surfaces, especially oligoclase; the proportion of solutes acquired by spring waters in contact with saprolitic plagioclases along the weathering front is assumed to be insignificant. The oligoclase weathering rates (W_{Pl}) were within the interval $(2.5 \pm 1.2) \times 10^{-14}$ mol

Appendix A

The identification code of the sampled and analyzed springs (Sample #) is given in Column 1. The results from the hydrological analysis are presented in Columns 2–4. The pHs of the springs are listed in Column 5. The concentrations of the dissolved species are given in brackets in Columns 6–15, and their concomitant activities, calculated using the Davies equation, are given in braces in Columns 16–20. The calculation of $\{Al^{3+}\}$ at 15 °C is based on hydrolysis constants for Al^{3+} in Nordstrom et al. (1990).

Sample #	Equivalent spring order (sampled from Fig. 5)	Catchment area (km^2) Eq. (15)	Travel time (years) Eq. (16)	pH	$[Na^+]$ (μM)	$[K^+]$ (μM)	$[Mg^{2+}]$ (μM)	$[Ca^{2+}]$ (μM)	$[HCO_3^-]$ (μM)	$[Cl^-]$ (μM)	$[SO_4^{2-}]$ (μM)	$[NO_3^-]$ (μM)	$[H_4SiO_4^0]$ (μM)	[Al] (μM)	$\{Na^+\}$	$\{Ca^{2+}\}$	$\{Al^{3+}\}$ 15°C	$\{H_4SiO_4^0\}$	$\{HCO_3^-\}$
1009	1.91	1.71	1.64	5.28	193	7.9	4.8	11	75	189	8.2	11.5	250	1.74	1.89E−04	1.02E−05	6.1E−07	2.50E−04	7.40E−05
1038	3.00	8.61	2.75	6.4	331	13.1	9.6	20	156	283	5.9	1.9	314	0.74	3.23E−04	1.80E−05	3.5E−09	3.14E−04	1.52E−04
1040	2.31	3.11	1.87	5.78	360	25.4	16.9	26	170	315	8.4	1.3	342	1.04	3.51E−04	2.34E−05	9.4E−08	3.42E−04	1.66E−04
1043	2.95	8.01	2.65	6.5	361	20.0	27.7	55	197	282	27.1	33.9	437		3.51E−04	4.87E−05		4.37E−04	1.91E−04
1048	3.53	19.14	4.43	5.09	395	16.2	39.8	33	74	389	59.4	19.4	283	0.22	3.83E−04	2.95E−05	9.8E−08	2.83E−04	7.16E−05
1077	2.31	3.11	1.87	6.70	259	39.0	24.5	73	303	225	10.2		316	0.30	2.52E−04	6.53E−05	1.7E−10	3.16E−04	2.95E−04
1415	2.35	3.28	1.90	6.12	265	19.0	30.4	61	238	159	2.9	56.0	330	0.15	2.58E−04	5.46E−05	3.3E−09	3.30E−04	2.31E−04
1430	1.46	0.87	1.51	6.25	201	7.9	15.0	24	131	138	7.3		171	0.37	1.97E−04	2.21E−05	4.3E−09	1.71E−04	1.28E−04
1433	1.99	1.91	1.68	6.67	303	21.0	33.8	42	251	158	6.1	38.4	323	1.04	2.95E−04	3.80E−05	7.5E−10	3.23E−04	2.45E−04
1442	1.59	1.06	1.54	5.38	173	21.8	15.8	32	92	135	8.0	27.1	160	0.41	1.69E−04	2.97E−05	1.2E−07	1.60E−04	8.99E−05
1446	1.89	1.65	1.63	6.00	165	1.0	10.8	17	86	134	7.2		107	0.37	1.62E−04	1.53E−05	1.4E−08	1.07E−04	8.42E−05
1449	1.79	1.43	1.60	5.04	129	3.1	10.8	17	51	100	7.3	35.5	118	2.85	1.27E−04	1.61E−05	1.5E−06	1.18E−04	5.03E−05
1468	1.60	1.07	1.54	5.7	213	4.0	8.0	18	121	114	6.0	0.0	233	1.56	2.09E−04	1.62E−05	1.70E−07	2.33E−04	1.19E−04
1477	1.72	1.29	1.58	5.43	188	7.7	34.6	35	183	100	7.7	0.3	241	1.48	1.84E−04	3.20E−05	3.8E−07	2.41E−04	1.79E−04
1490	1.93	1.77	1.65	5.7	207	8.0	23.0	40	171	138	6.0	0.0	248	1.85	2.03E−04	3.61E−05	2.21E−07	2.48E−04	1.68E−04
1491	2.10	2.27	1.73	5.69	261	18.5	31.7	67	267	146	4.2		317	1.00	2.54E−04	6.03E−05	1.2E−07	3.17E−04	2.60E−04
1611	1.77	1.39	1.59	5.3	193	10.0	28.0	32	86	130	33.0	26.0	163	0.37	1.89E−04	2.92E−05	1.19E−07	1.63E−04	8.41E−05
1612	1.39	0.78	1.50	5.52	336	13.1	18.3	27	163	191	12.1	16.9	264	0.15	3.28E−04	2.45E−05	3.0E−08	2.64E−04	1.59E−04
1613	1.70	1.25	1.57	6.47	509	25.4	28.8	49	346	207	22.7	25.5	451		4.94E−04	4.33E−05		4.51E−04	3.35E−04
1615	1.47	0.88	1.51	5.38	281	24.6	27.1	25	169	179	19.6	0.3	215	0.70	2.74E−04	2.22E−05	2.0E−07	2.15E−04	1.65E−04
1622	1.15	0.55	1.46	5.73	192	40.3	21.3	18	135	136	2.4	17.7	199		1.88E−04	1.66E−05		1.99E−04	1.32E−04
1625	1.79	1.42	1.60	6.04	286	8.7	12.5	9	116	173	13.8		261		2.80E−04	7.80E−06		2.61E−04	1.14E−04
1626	1.28	0.67	1.48	5.68	439	10.0	28.3	53	292	243	6.6		464	0.19	4.26E−04	4.74E−05	2.3E−08	4.64E−04	2.84E−04
1628	1.10	0.51	1.45	6.37	398	31.8	34.6	67	314	243	8.0	0.8	322	0.26	3.86E−04	5.94E−05	1.5E−09	3.22E−04	3.05E−04
1629	1.70	1.25	1.57	6.17	313	44.4	32.9	50	323	146	5.2	2.4	362	0.19	3.05E−04	4.50E−05	3.2E−09	3.62E−04	3.14E−04
1631	1.05	0.47	1.45	6.38	371	25.6	30.4	59	331	197	3.0		366	0.19	3.60E−04	5.24E−05	1.0E−09	3.66E−04	3.22E−04
1632	1.32	0.70	1.48	5.39	254	20.5	17.5	21	139	180	2.3		227	0.93	2.49E−04	1.88E−05	2.6E−07	2.27E−04	1.36E−04
1649	1.76	1.37	1.59	5.58	368	16.2	22.9	34	253	210	9.5		406	0.26	3.59E−04	3.08E−05	4.4E−08	4.06E−04	2.46E−04
1652	2.90	7.50	2.57	5.11	245	8.2	22.9	14	81	216	9.4		161	1.22	2.40E−04	1.31E−05	5.5E−07	1.61E−04	7.94E−05
1659	1.34	0.73	1.49	5.10	328	22.6	64.2	83	122	326	51.7	74.5	140	1.48	3.18E−04	7.29E−05	6.3E−07	1.40E−04	1.19E−04
1663	1.59	1.06	1.54	5.67	259	11.5	24.6	35	123	161	20.7	54.2	240	0.44	2.52E−04	3.18E−05	5.8E−08	2.40E−04	1.20E−04
1664	1.86	1.58	1.62	5.71	363	15.6	32.5	32	246	235	12.6	1.9	256	0.33	3.54E−04	2.87E−05	3.8E−08	2.56E−04	2.40E−04
1665	1.96	1.84	1.66	5.28	295	14.1	20.0	33	203	175	4.0		335	0.70	2.88E−04	2.95E−05	2.4E−07	3.35E−04	1.98E−04
1667	3.66	23.04	5.06	5.41	371	14.9	21.3	21	178	244	17.9		328	0.33	3.62E−04	1.89E−05	8.7E−08	3.28E−04	1.74E−04
1670	1.59	1.06	1.54	5.44	197	8.2	17.5	14	91	154	4.5		199	0.85	1.94E−04	1.32E−05	2.1E−07	1.99E−04	8.89E−05
1675	2.59	4.70	2.12	5.75	432	26.2	43.8	59	295	251	12.9	35.6	367	0,.19	4.19E−04	5.24E−05	1.8E−08	3.67E−04	2.86E−04
1678	1.96	1.83	1.66	6.33	373	11.3	20.4	22	184	224	12.9	1.8	313	0.44	3.64E−04	1.94E−05	3.2E−09	3.13E−04	1.80E−04
1680	1.14	0.54	1.46	5.73	248	7.7	22.1	18	160	158	4.0	0.8	279	0.85	2.42E−04	1.67E−05	9.2E−08	2.79E−04	1.56E−04
1682	1.40	0.80	1.50	5.32	215	30.0	23.8	22	102	172	4.5	23.2	181	2.11	2.11E−04	2.04E−05	6.8E−07	1.81E−04	9.98E−05
1683	2.19	2.59	1.79	6.18	262	12.3	20.4	27	122	176	14.0	8.1	233	0.37	2.56E−04	2.44E−05	6.1E−09	2.33E−04	1.20E−04
1684	1.41	0.81	1.50	6.04	290	7.4	27.1	62	288	157	8.1		300	0.22	2.83E−04	5.53E−05	7.1E−09	3.00E−04	2.81E−04
1685	2.71	5.59	2.26	6.21	441	25.4	26.3	42	230	281	21.1	12.6	421	0.41	4.28E−04	3.69E−05	5.7E−09	4.21E−04	2.24E−04
1697	2.11	2.30	1.74	5.18	156	6.7	12.5	13	45	126	7.7	21.3	123	1.22	1.53E−04	1.21E−05	5.1E−07	1.23E−04	4.46E−05
1701	2.26	2.88	1.83	5.30	207	9.2	23.3	33	93	153	26.3	9.0	163	1.07	2.02E−04	2.99E−05	3.6E−07	1.63E−04	9.10E−05
1703	3.59	20.68	4.68	5.69	306	12.6	29.6	55	164	204	29.5	19.2	246	0.30	2.97E−04	4.94E−05	3.6E−08	2.46E−04	1.60E−04
1707	2.70	5.54	2.26	5.23	307	35.4	34.2	42	180	230	5.6	47.9	235	1.22	2.99E−04	3.73E−05	4.5E−07	2.35E−04	1.75E−04
1708	1.40	0.80	1.50	6.23	365	13.3	36.7	57	248	214	12.5	22.6	299	0.07	3.55E−04	5.04E−05	9.4E−10	2.99E−04	2.41E−04
1709	1.07	0.49	1.45	6.19	334	16.9	28.3	45	237	232	14.4		307	0.30	3.25E−04	4.04E−05	4.6E−09	3.07E−04	2.30E−04
2003	2.63	5.01	2.17	7.18	194	17.6	44.2	34	104	149	51.8	35.0	187		1.89E−04	3.04E−05		1.87E−04	1.02E−04
2019	2.42	3.67	1.96	6.75	324	22.5	21.7	41	257	198	9.6		350	2.05	3.16E−04	3.65E−05	7.9E−10	3.50E−04	2.51E−04
2022	1.36	0.75	1.49	5.86	261	8.8	15.8	32	145	166	12.0	5.0	285		2.55E−04	2.91E−05		2.85E−04	1.42E−04

Appendix A (*continued*)

Sample #	Equivalent spring order (sampled from Fig. 5)	Catchment area (km^2) Eq. (15)	Travel time (years) Eq. (16)	pH	$[Na^+]$ (μM)	$[K^+]$ (μM)	$[Mg^{2+}]$ (μM)	$[Ca^{2+}]$ (μM)	$[HCO_3^-]$ (μM)	$[Cl^-]$ (μM)	$[SO_4^{2-}]$ (μM)	$[NO_3^-]$ (μM)	$[H_4SiO_4^0]$ (μM)	[Al] (μM)	$\{Na^+\}$	$\{Ca^{2+}\}$	$\{Al^{3+}\}$ 15°C	$\{H_4SiO_4^0\}$	$\{HCO_3^-\}$
2033	1.24	0.63	1.47	5.15	145	10.2	38.6	50	182	108	16.3		171		1.42E−04	4.52E−05		1.71E−04	1.78E−04
2035	2.81	6.48	2.41	5.29	330	3.2	27.1	26	220	195	11.4		424	1.20	3.21E−04	2.35E−05	4.0E−07	4.24E−04	2.14E−04
2039	1.31	0.70	1.48	5.60	246	24.5	32.3	51	250	134	9.4	26.5	349		2.40E−04	4.58E−05		3.49E−04	2.44E−04
2042	1.03	0.46	1.44	5.52	239	11.2	12.7	14	146	169	4.7		247		2.34E−04	1.33E−05		2.47E−04	1.43E−04
2044	1.54	0.98	1.53	5.82	183	3.2	7.3	10	81	134	8.5		195		1.79E−04	8.90E−06		1.95E−04	8.00E−05
2049	1.57	1.03	1.53	5.11	162	14.2	19.6	24	64	143	20.6	21.1	151	1.41	1.59E−04	2.24E−05	6.4E−07	1.51E−04	6.25E−05
2054	1.15	0.55	1.46	4.55	227	23.5	15.7	7	106	195	9.8		241		2.23E−04	6.57E−06		2.41E−04	1.04E−04
2055	1.04	0.47	1.44	4.90	236	34.5	29.0	62	206	178	23.4	5.0	310		2.30E−04	5.59E−05		3.10E−04	2.01E−04
2070	1.08	0.50	1.45	6.71	357	16.8	25.4	27	219	197	8.3		379	2.92	3.48E−04	2.47E−05	1.5E−09	3.79E−04	2.14E−04
2079	2.87	7.08	2.50	6.43	339	25.5	10.4	34	265	119	12.4		455	2.89	3.31E−04	3.06E−05	1.1E−08	4.55E−04	2.59E−04
2089	1.96	1.85	1.67	6.15	403	19.1	18.3	27	295	199	9.1		588	1.53	3.92E−04	2.45E−05	2.9E−08	5.88E−04	2.87E−04
2091	1.18	0.57	1.46	5.92	274	8.3	18.3	46	223	163	8.8		332	1.31	2.68E−04	4.14E−05	7.0E−08	3.32E−04	2.17E−04
2095	1.95	1.81	1.66	5.98	280	28.0	68.0	106	460	128	16.0		297		2.71E−04	9.32E−05		2.97E−04	4.45E−04
2101	3.02	8.94	2.80	6.08	296	24.3	21.3	24	142	216	10.5		266	1.97	2.89E−04	2.18E−05	5.3E−08	2.66E−04	1.39E−04
2102	2.76	6.08	2.34	5.57	277	21.2	22.5	30	131	221	4.9		245		2.70E−04	2.68E−05		2.45E−04	1.28E−04
2801	4.77	121.27	20.77	5.69	209	17.7	19.3	15	128	141	4.5	1.3	290		2.05E−04	1.36E−05		2.90E−04	1.25E−04
2810	1.20	0.60	1.47	5.36	291	11.5	21.9	24	118	248	10.7		348		2.85E−04	2.21E−05		3.48E−04	1.15E−04
2811	1.00	0.44	1.44	5.82	133	2.9	11.3	10	40	96	7.6	7.7	121		1.31E−04	9.64E−06		1.21E−04	3.92E−05
2829	1.07	0.49	1.45	5.62	221	23.6	47.8	44	214	161	16.6		369		2.15E−04	3.96E−05		3.69E−04	2.09E−04
2839	1.25	0.64	1.47	5.50	191	11.6	15.3	12	92	141	4.6		203		1.88E−04	1.07E−05		2.03E−04	9.07E−05
2842	2.03	2.03	1.69	5.10	172	10.7	24.1	17	72	149	11.5	29.0	181	1.49	1.69E−04	1.57E−05	6.9E−07	1.81E−04	7.04E−05
2851	1.68	1.22	1.56	6.12	294	17.2	28.6	32	165	169	16.6		427		2.87E−04	2.93E−05		4.27E−04	1.61E−04
2853	1.52	0.95	1.52	5.59	252	21.5	23.0	16	105	237	7.2		321		2.46E−04	1.51E−05		3.21E−04	1.02E−04
2854	2.78	6.25	2.37	6.38	284	25.7	18.0	15	179	183	5.1		434		2.78E−04	1.34E−05		4.34E−04	1.75E−04
2855	1.00	0.44	1.44	5.55	157	11.4	12.3	16	98	96	8.4		233	1.67	1.54E−04	1.53E−05	3.2E−07	2.33E−04	9.63E−05
2857	1.80	1.46	1.60	6.16	195	5.7	15.5	16	85	152	8.2		241		1.91E−04	1.48E−05		2.41E−04	8.29E−05
2859	1.04	0.47	1.44	5.25	160	10.7	16.9	27	67	130	22.5	21.0	194	4.07	1.57E−04	2.51E−05	1.5E−06	1.94E−04	6.53E−05
2868	1.79	1.42	1.60	5.67	328	36.4	33.3	46	158	273	25.1		331	1.19	3.19E−04	4.15E−05	1.5E−07	3.31E−04	1.54E−04
2870	1.11	0.52	1.45	5.51	306	12.8	20.9	13	105	228	10.6		330	2.07	2.99E−04	1.23E−05	4.3E−07	3.30E−04	1.03E−04
2871	2.18	2.54	1.78	5.55	249	13.1	18.9	14	108	158	11.7		322		2.44E−04	1.28E−05		3.22E−04	1.05E−04
2872	2.87	7.08	2.50	5.55	384	17.5	25.8	20	150	259	11.5		376		3.74E−04	1.78E−05		3.76E−04	1.46E−04
2873	2.01	1.97	1.68	5.45	292	21.2	17.7	22	153	200	4.2		449	2.37	2.86E−04	1.99E−05	5.7E−07	4.49E−04	1.50E−04
2874	1.03	0.46	1.44	5.39	206	15.6	20.3	13	93	166	7.8		254		2.02E−04	1.17E−05		2.54E−04	9.09E−05
2876	1.26	0.65	1.47	5.74	290	22.2	25.7	19	166	197	6.4		398	1.26	2.83E−04	1.76E−05	1.3E−07	3.98E−04	1.62E−04
2882	5.04	180.91	30.32	5.47	263	15.2	20.7	27	155	163	3.7		435	2.52	2.57E−04	2.48E−05	5.8E−07	4.35E−04	1.51E−04
2884	2.35	3.29	1.90	5.72	212	14.0	18.9	17	96	175	3.7		307	1.19	2.08E−04	1.58E−05	1.3E−07	3.07E−04	9.44E−05
Median	1.77	1.39	1.59	5.69	265	16	23	27	156	175	9	18	290	1.0	2.58E−04	2.47E−05	9.36E−08	2.90E−04	1.52E−04
Average	1.92	6.21	2.36	5.74	274	17	24	32	169	185	12	19	288	1.1	2.67E−04	2.93E−05	2.24E−07	2.88E−04	1.64E−04
St.dev.	0.81	23.17	3.71	0.49	80	9	11	19	82	55	10	18	96	0.9	7.76E−05	1.66E−05	3.17E−07	9.57E−05	7.90E−05
Minimum	1.0	0.4	1.4	4.6	129	1	7	7	40	96	2		107	0.1	1.27E−04	6.57E−06	1.69E−10	1.07E−04	3.92E−05
Maximum	5.0	180.9	30.3	7.2	509	44	68	106	460	389	59	75	588	4.1	4.94E−04	9.32E−05	1.50E−06	5.88E−04	4.45E−04

Appendix B

The identification code of the sampled and analyzed springs (Sample #) is given in Column 1. Column 2 reports the annual rainfall in the vicinity of the spring sites (in agreement with Fig. 1). Colums 3–7 summarize the results of the SiB model (Van der Weijden and Pacheco, 2006): x is the anorthite fraction of plagioclase assumed in the model, indicating a compositional range from albite to oligoclase, [Pl] is the contribution of plagioclase dissolution to the water chemistry, whereas [smectite], [halloysite] and [gibbsite] are the calculated amounts of aluminosilicate and aluminum hydroxide phases precipitated along the flow path. Columns 8–14 list the results of the thermodynamic analyses: the Q-values (ion activity products) were calculated from the relevant activities of the species involved in the equilibria of the secondary solid phases. The concomitant K_{eq} values in Columns 8–10 were adopted from Nordstrom et al. (1990), the ones in Columns 11–13 from Langmuir (1997). The ΔG_r values in Column 14, pertaining to the congruent dissolution of the plagioclases (reaction (R1)), were calculated using the relation: $\Delta G_r = 2.303RT(\log Q - \log K_{eq})$, where R is the gas constant (in kJ mol^{-1} K^{-1}) and T the temperature (in K), Q is the actual ion activity product of the species involved in the dissolution reaction, and $\log K_{eq} = -\Delta G_r^0/2.303RT$. The ΔG_r^0 values for reaction (R1) were calculated from the ΔG_f^0 values of the plagioclases (with x as in Column 3) and the concomitant dissolved species as given in Anderson (1996) and Faure (1998). All values were calculated for 15 °C by application of the Van 't Hoff equation using the enthalpies of the dissolution reactions (ΔH_r^0) derived from the ΔH_f^0 values listed in the two last mentioned textbooks. The final column gives the weathering rates calculated as explained in the text.

Sample #	P (mm year^{-1})	x	[Pl] (mM)	[Smectite] (μM)	[Halloysite] (μM)	[Gibbsite] (μM)	Q/K_{eq} amorphous $Al(OH)_3$	Q/K_{eq} microcrystalline gibbsite	Q/K_{eq} crystalline gibbsite	Q/K_{eq} allophane	Q/K_{eq} halloysite	Q/K_{eq} kaolinite	ΔG_r (kJ mol^{-1})	$W_{Pl} \times 10^{-13}$ (mol m^{-2} s^{-1})
1009	1246	0.1	95	0	16	36	0.014	0.5	34	0.8	0.9	83	−20.7	0.169
1038	1253	0.1	171	0	94	0	0.190	6.0	446	5.8	14.7	1379	−4.2	0.182
1040	1235	0.1	186	0	102	0	0.069	2.2	163	2.5	5.8	548	−9.8	0.292
1043	1176	0.1	202	0	78	33								0.223
1048	1117	0.1	99	0	5	49	0.001	0.0	1	0.2	0.0	4	−27.6	0.065
1077	1270	0.25	188	0	117	0	0.072	2.3	169	3.5	5.6	524	−17.6	0.294
1415	898	0.1	168	0	92	0	0.025	0.8	60	1.6	2.1	194	−11.1	0.259
1430	893	0.15	93	0	54	0	0.081	2.6	190	2.5	3.4	320	−17.4	0.181
1433	895	0.15	173	0	100	0	0.259	8.2	607	8.2	20.5	1927	−6.2	0.303
1442	894	0.1	89	0	49	0	0.005	0.2	13	0.4	0.2	20	−25.8	0.169
1446	839	0.2	64	0	38	0	0.049	1.5	114	1.4	1.3	120	−28.5	0.115
1449	877	0.1	52	0	17	11	0.006	0.2	15	0.4	0.2	18	−30.3	0.095
1468	870	0.1	115	0	51	13	0.089	2.8	209	2.4	5.1	480	−13.4	0.219
1477	869	0.2	145	0	87	0	0.025	0.8	58	1.1	1.5	138	−28.1	0.269
1490	933	0.15	142	0	82	0	0.094	3.0	221	2.5	5.8	541	−17.7	0.252
1491	932	0.25	202	0	126	0	0.049	1.5	114	1.9	3.8	355	−25.7	0.340
1611	953	0.1	89	0	49	0	0.004	0.1	9	0.4	0.1	14	−26.8	0.164
1612	1143	0.1	142	0	78	0	0.004	0.1	9	0.5	0.2	22	−21.1	0.278
1613	1148	0.2	241	0	130	14								0.450
1615	1193	0.1	102	0	56	0	0.009	0.3	22	0.6	0.5	46	−21.4	0.198
1622	1207	0.1	104	0	57	0								0.209
1625	1010	0.1	85	0	0	47								0.156
1626	1034	0.1	248	0	136	0	0.009	0.3	20	0.9	1.0	92	−13.2	0.492
1628	1079	0.3	211	0	137	0	0.065	2.0	152	2.9	5.1	481	−22.7	0.425
1629	1075	0.25	192	0	108	12	0.035	1.1	82	2.0	3.1	293	−22.4	0.358
1631	1050	0.25	224	0	140	0	0.047	1.5	109	2.5	4.2	394	−19.6	0.453
1632	1017	0.1	123	0	68	0	0.013	0.4	30	0.8	0.7	68	−20.3	0.244
1649	1156	0.1	222	0	122	0	0.008	0.3	19	0.9	0.8	77	−15.4	0.410
1652	1109	0.1	83	0	41	5	0.004	0.1	9	0.4	0.2	15	−27.6	0.095
1659	1073	0.1	61	0	34	0	0.004	0.1	10	0.3	0.1	14	−27.5	0.120
1663	1030	0.1	124	0	62	7	0.020	0.6	47	1.1	1.2	112	−16.9	0.237

1664	1027	0.15	222	46	89	0	0.017	0.5	41	1.0	1.1	103	−21.0	0.400
1665	1005	0.1	184	0	101	0	0.006	0.2	13	0.6	0.5	44	−20.0	0.324
1667	1064	0.1	180	0	99	0	0.005	0.2	12	0.6	0.4	38	−19.3	0.104
1670	980	0.1	93	0	36	15	0.015	0.5	36	0.8	0.7	70	−21.1	0.177
1675	892	0.15	189	0	109	0	0.011	0.3	26	1.0	1.0	93	−19.0	0.261
1678	932	0.1	173	0	95	0	0.107	3.4	252	3.9	8.2	774	−5.9	0.305
1680	923	0.1	154	0	85	0	0.049	1.5	114	1.9	3.3	312	−13.4	0.310
1682	948	0.1	100	0	55	0	0.021	0.7	49	0.9	0.9	88	−21.3	0.196
1683	976	0.1	128	0	70	0	0.072	2.3	169	2.6	4.1	387	−10.7	0.210
1684	918	0.3	205	0	133	0	0.032	1.0	75	1.7	2.3	220	−28.3	0.400
1685	960	0.1	232	0	128	0	0.083	2.6	194	3.6	8.6	804	−4.8	0.300
1697	946	0.1	49	0	11	16	0.006	0.2	14	0.4	0.2	17	−29.0	0.083
1701	902	0.1	90	0	50	0	0.010	0.3	23	0.6	0.4	36	−24.2	0.145
1703	907	0.1	127	0	70	0	0.014	0.5	34	0.9	0.9	81	−17.0	0.079
1707	886	0.1	114	0	63	0	0.007	0.2	18	0.6	0.4	41	−21.9	0.148
1708	897	0.25	192	0	120	0	0.016	0.5	37	1.1	1.1	107	−25.3	0.375
1709	891	0.15	168	0	97	0	0.058	1.8	137	2.5	4.4	414	−13.4	0.340
2003	1154	0.1	103	0	57	0								0.139
2019	1095	0.15	197	0	113	0	0.473	15.0	1110	13.2	40.7	3822	−3.3	0.294
2022	1111	0.1	148	0	73	8								0.290
2033	1225	0.3	150	12	88	0								0.298
2035	1169	0.1	199	0	77	33	0.010	0.3	24	0.9	1.0	99	−16.6	0.242
2039	1204	0.1	178	0	98	0								0.352
2042	1117	0.1	137	0	75	0								0.278
2044	1110	0.1	79	0	17	26								0.152
2049	1079	0.1	77	0	38	4	0.005	0.1	11	0.4	0.2	16	−28.4	0.146
2054	1089	0.1	100	0	28	28								0.201
2055	1087	0.1	164	0	90	0								0.332
2070	1195	0.1	211	0	116	0	0.704	22.3	1651	17.2	65.5	6158	2.6	0.425
2079	1164	0.1	253	0	139	0	0.753	23.8	1766	15.9	84.2	7912	2.3	0.296
2089	1184	0.1	273	0	105	45	0.280	8.9	657	8.2	40.4	3796	0.1	0.480
2091	1083	0.1	176	0	97	0	0.137	4.3	321	3.8	11.2	1051	−7.8	0.353
2095	1197	0.3	395	93	180	0			0					0.696
2101	1059	0.1	146	0	80	0	0.312	9.9	730	6.1	20.3	1909	−6.3	0.153
2102	1053	0.1	135	0	74	0								0.169
2801	1165	0.1	141	0	62	15								0.020
2810	1328	0.1	119	0	0	66								0.238
2811	1412	0.1	43	0	2	21								0.088
2829	1208	0.1	204	0	112	0								0.413
2839	1262	0.1	99	0	43	11								0.197
2842	1454	0.1	79	0	26	17	0.005	0.1	11	0.4	0.2	20	−27.2	0.137
2851	1246	0.1	180	0	50	50								0.337
2853	977	0.1	118	0	13	52								0.226
2854	1192	0.1	141	0	0	77								0.174
2855	1270	0.1	103	0	34	23	0.048	1.5	113	1.6	2.7	258	−16.8	0.209
2857	1240	0.1	86	0	5	42	0.000							0.157
2859	1491	0.1	74	0	12	29	0.029	0.9	67	1.0	1.4	128	−21.0	0.151
2868	1282	0.1	180	0	99	0	0.053	1.7	125	2.1	4.3	406	−11.5	0.331

(*continued on next page*)

Appendix (*continued*)

Sample #	P (mm year^{-1})	x	[Pl] (mM)	[Smectite] (μM)	[Halloysite] (μM)	[Gibbsite] (μM)	Q/K_{eq} amorphous $Al(OH)_3$	Q/K_{eq} microcrystalline gibbsite	Q/K_{eq} crystalline gibbsite	Q/K_{eq} allophane	Q/K_{eq} halloysite	Q/K_{eq} kaolinite	ΔG_r (kJ mol^{-1})	$W_{Pl} \times 10^{-13}$ (mol m^{-2} s^{-1})
2870	1151	0.1	117	0	6	58	0.050	1.6	116	1.9	4.0	378	−13.1	0.236
2871	1104	0.1	119	0	13	52								0.196
2872	1103	0.1	166	0	55	37								0.194
2873	1163	0.1	166	0	18	73	0.043	1.4	102	2.0	4.8	450	−11.7	0.288
2874	1342	0.1	106	0	29	29		0.0		0.0	0.0			0.215
2876	1205	0.1	176	0	58	39	0.074	2.3	173	2.8	7.2	679	−9.4	0.349
2882	1358	0.1	168	0	28	65	0.051	1.6	119	2.2	5.4	507	−11.5	0.016
2884	1254	0.1	108	0	6	54	0.065	2.1	153	2.3	4.9	463	−12.3	0.167
Median		0.10	142	0	70	0	0.030	1.0	71	1.5	1.8	194	−17.7	0.236
Average		0.13	148	2	68	14	0.079	2.5	184	2.5	6.9	655	−17.2	0.247
St. dev.		0.06	59	11	42	21	0.146	4.6	343	3.4	14.9	1408	8.4	0.118

$m^{-2}\ s^{-1}$, which is very close to the range of rates determined in granite environments under field conditions in other studies (White and Brantley, 2003; among others). In general, the waters collected at the spring sites in the Vouga granites were in equilibrium with microcrystalline gibbsite and(or) halloysite/allophane, and undersaturated with respect to albite-oligoclase. The range of the calculated dissolution rates was, at least in part, caused by the fact that the spring waters consist of packets of water that are exposed to different pathways and travel times that have been in contact with fresh and weathered oligoclases.

References

Anderson, G.M., 1996. Thermodynamics of Natural Systems. John Wiley & Sons, Inc., New York (382 pp).

Appelo, C.A.J., Postma, D., 2005. Geochemistry, Groundwater and Pollution. A.A. Balkema, Rotterdam, 649pp.

Arvidson, R.S., Lüttge, A., 2010. Mineral dissolution kinetics as a function of distance from equilibrium—New experimental results. Chem. Geol. 269, 79–88.

Beig, M.S., Lüttge, A., 2006. Albite dissolution kinetics as a function of distance from equilibrium: implications for natural feldspar weathering. Geochim. Cosmochim. Acta 70, 1402–1420.

Berner, R.A., Lasaga, A.C., Garrels, R.M., 1983. The carbonate–silicate geochemical cycle and its effect on atmospheric carbon dioxide over the past 100 Million years. Am. J. Sci. 283, 641–683.

Blum, A.E., 1994. Feldspars in weathering. In: Parson, I. (Ed.), Feldspars and Their Reactions. Kluwer Academic Publishers, Dordrecht, The Netherlands, pp. 595–630.

Bolin, B., Rodhe, H., 1973. A note on the concepts of age distribution and transit time in natural reservoirs. Tellus 25 (1), 58–62.

Boussinesq, J., 1877. Essai sur la théorie des eaux courantes. Mem. Acad. Sci. Inst. Fr. 23, 252–260.

Boussinesq, J., 1903. Sur le débit, en temps de sécheresse, d'une source alimentée par une nappe d'eaux d'infiltration. CR Hebd. Seanc. Acad. Sci. Paris 136, 1511–1517.

Boussinesq, J., 1904. Recherches théoriques sur l'écoulement des nappes d'eau infiltrées dans le sol et sur débit de sources. J. Math. Pures Appl. 10, 5–78.

Brantley, S.L., Mellott, N.P., 2000. Surface area and porosity of primary silicate minerals. Am. Mineral. 58, 1767–1783.

Brantley, S.L., White, A.F., Hodson, M.E., 1999. Surface area of primary silicate minerals. In: Jamtveit, B., Meakin, P. (Eds.), Growth Dissolution and Pattern Formation in Geosystems. Kluwer Academic Publishers, pp. 291–326 (Chapter 14).

Brutsaert, W., 1994. The unit response of groundwater outflow from a hillslope. Water Resour. Res. 34, 233–240.

Brutsaert, W., Lopez, J.P., 1998. Basin-scale geohydrologic drought flow features of riparian aquifers of the southern Great Plains. Water Resour. Res. 30, 2759–2763.

Brutsaert, W., Nieber, J.L., 1977. Regionalized drought flow hydrographs from a mature glaciated plateau. Water Resour. Res. 13, 637–643.

Burch, T.E., Nagy, K.L., Lasaga, A.C., 1993. Free energy dependence of albite dissolution kinetics at 80 °C and pH 8.8. Chem. Geol. 105, 137–162.

Caetano, C.A.R., Pacheco, F.A.L., 2008. Modelação de escoamentos fluviais na região de Trás-os-Montes e Alto Douro utilizando o modelo SWAT. In: V Seminário Recursos Geológicos, Ambiente e Ordenamento do Território, UTAD, Vila Real, 16–18 October 2008. Special Volume in CD-ROM, p. 44–53.

Cooper, H.H. Jr., Rorabaugh, M.I., 1963. Groundwater Movements and Bank Storage Due to Flood Stages in Surface Streams. USGS Water Supply Paper 1536-J: 343–366.

De Bartolo, S.G., Gabriele, S., Gaudio, R., 2000. Multifractal behaviour of river networks. Hydrol. Earth Syst. Sci. 4 (1), 105–112.

De Bartolo, S.G., Gaudio, R., Gabriele, S., 2004. Multifractal analysis of river networks: a sand-box approach. Water Resour. Res. 40, 1–10.

De Bartolo, S.G., Veltri, M., Primavera, L., 2006. Estimated generalized dimensions of river networks. J. Hydrol. 322, 181–191.

Domenico, P.A., Schwartz, F.W., 1990. Physical and Chemical Hydrogeology. John Wiley & Sons Inc., New York, 824pp.

Drever, J.I., 1997. Weathering processes. In: Saether, P.M., de Caritat, P. (Eds.), Geochemical Processes, Weathering and Groundwater Recharge in Catchments. A.A. Balkema, Rotterdam/Brookfield, pp. 3–19.

Drever, J.I., Clow, D.W., 1995. Weathering rates in catchments. In: White, A.F., Brantley, S.L. (Eds.), Chemical Weathering Rates of Silicate Minerals, Reviews in Mineralogy, vol. 31. Mineralogical Society of America, Washington, DC, USA, pp. 463–483.

Dupré, B., Dessert, C., Oliva, P., Goddéris, Y., Viers, J., François, L., Millot, R., Gaillardet, J., 2003. Rivers, chemical weathering and Earth's climate. CR Geosci. 335, 1141–1160.

ESRI, 2007. ArcMap (version 9.3). New York St., Redlands, USA, 131p.

ESRI, 2009. ArcHydro Tools – Tutorial (version 1.3). New York St., Redlands, USA, 131p.

Etcheverry, D., Perrochet, P., 2000. Direct simulation of groundwater transit-time distributions using the reservoir theory. Hydrogeol. J. 8 (2), 200–208.

Faure, G., 1998. Principles and Applications of Geochemistry, second ed. Prentice Hall, Upper Saddle River, NJ, USA, 600pp.
Gaudio, R., De Bartolo, S.G., Primavera, L., Gabriele, S., Veltri, M., 2006. Lithologic control on the multifractal spectrum of river networks. J. Hydrol. 327, 365–375.
Goddéris, Y., Francois, L.M., Probst, A., Schott, J., Moncoulon, D., Labat, D., Viville, D., 2006. Modelling weathering processes at the catchment scale: the WITCH numerical model. Geochim. Cosmochim. Acta 70, 1128–1147.
Goddéris, Y., Roelandt, C., Schott, J., Pierret, M.C., Francois, L.M., 2009. Towards an integrated model of weathering, climate, and biospheric processes. In: Oelkers, E.H., Schott, J. (Eds.), Thermodynamics and Kinetics of Water–Rock Interaction, vol. 70. Mineralogical Soc Amer., pp. 411–434.
Godinho, M.M., 1980. O Plutonito do Caramulo. Memórias e Notícias, publicações do Museu e Laboratório Mineralógico e Geológico da Universidade de Coimbra, 89/90, 269pp.
Griffiths, G.A., Clausen, B., 1997. Streamflow recession in basins with multiple water storages. J. Hydrol. 190, 60–74.
Hartmann, J., Jansen, N., Dürr, H.H., Kempe, S., Köhler, P., 2009. Global CO_2-consumption by chemical weathering: What is the contribution of highly active weathering regions? Global Planet. Change 69, 185–194.
Helgeson, H.C., Garrels, R.M., Mackenzie, F.T., 1969. Evaluation of irreversible reactions in geochemical processes involving minerals and aqueous solutions—II. Applications. Geochim. Cosmochim. Acta 33, 455–481.
Hellmann, R., Tisserand, D., 2006. Dissolution kinetics as a function of the Gibbs free energy of reaction: an experimental study based on albite feldspar. Geochim. Cosmochim. Acta 70, 364–383.
Hornberger, G.M., Beven, K.J., Germann, P.E., 1990. Interferences about solute transport in macroporous forest soils from time series models. Geoderma 46, 249–262.
Horton, R.E., 1945. Erosional development of streams and their drainage basins: hydrophysical approach to quantitative morphology. Geol. Soc. Am. Bull. 56, 275–370.
La Barbera, P., Rosso, R., 1987. Fractal geometry of river networks. Trans. Am. Geophys. Union 68, 1276.
La Barbera, P., Rosso, R., 1989. On the fractal dimension of stream networks. Water Resour. Res. 25, 735–741.
Langmuir, D., 1997. Aqueous Environmental Geochemistry. Prentice Hall, Upper saddle River, New Jersey, USA, 600pp.
Lasaga, A.C., 1998. Kinetic theory in the earth sciences. In: Holland, H.D. (Ed.), Princeton Series in Geochemistry. Princeton University Press, Princeton, New Jersey, p. 811.
Lasaga, A.C., Lüttge, A., 2004. Mineralogical approaches to fundamental crystal dissolution kinetics—dissolution of an A_3B structure. Eur. J. Mineral. 16, 713–729.
Lüttge, A., 2005. Etch pit coalescence, surface area, and overall mineral dissolution rates. Am. Mineral. 90, 1767–1783.
Lüttge, A., 2006. Crystal dissolution kinetics and Gibbs free energy. J. Electron. Spectrosc. Relat. Phenom. 150, 248–259.
Maher, K., 2010. The dependence of chemical weathering rates on fluid residence time. Earth Planet. Sci. Lett. 294, 101–110.
Maher, K., Steefel, C.I., White, A.F., Stonestrom, D.A., 2009. The role of reaction affinity and secondary minerals in regulating chemical weathering rates at the Santa Cruz Soil Chronosequence, California. Geochim. Cosmochim. Acta 73, 2804–2831.
Malvicini, C.F., Steenhuis, T.S., Walter, M.T., Parlange, J.-Y., Walter, M.F., 2005. Evaluation of spring flow in the uplands of Matalom, Leyte, Philippines. Adv. Water Resour. 28, 1083–1090.
Martins, 1985. Caracterização sumária dos solos de Trás-os-Montes e Alto Douro e sua ocupação. Technical Report, Instituto Universitário de Trás-os-Montes e Alto Douro, 30pp.
Martins, A.A.A., Madeira, M.V., Refega, A.A.G., 1995. Influence of rainfall on properties of soils developed on granite in Portugal. Arid Soil Res. Rehabil. 9, 353–366.
McGuire, K.J., McDonnell, J.J., 2006. A review and evaluation of catchment transit time modelling. J. Hydrol. 330, 543–563.
Medina, J.M.P.G., 1996. Contribuição para o Conhecimento da Geologia do Grupo das Beiras (CXG) na Região do Caramulo–Buçaco (Portugal Central). PhD thesis, University of Aveiro, 183 pp.
Mendoza, G.F., Steenhuis, T.S., Walter, M.T., Parlange, J.Y., 2003. Estimating basin-wide hydraulic parameters of a semi-arid mountainous watershed by recession flow analysis. J. Hydrol. 279, 57–69.
Meunier, A., Sardini, P., Robinet, J.C., Prêt, D., 2007. The petrography of weathering processes: facts and outlooks. Clay Miner. 42, 415–435.
Meyboom, P., 1961. Estimating groundwater recharge from stream hydrographs. J. Geophys. Res. 66, 1203–1214.
Nikora, V.I., Sapozhnikov, V.B., 1993. River network fractal geometry and its computer simulation. Water Resour. Res. 29, 3565–3575.
Nordstrom, D.K., Plummer, L.N., Langmuir, D., Busenberg, E., May, H.M., Jones, B.F., Parkhurst, D.L., 1990. Revised chemical equilibrium data for major water–mineral reactions and their limitations. In: Melchior, D.C., Bassett, R.L. (Eds.), Chemical Modeling of Aqueous Systems II. ACS Symposium Series 416. American Chemical Society, Washington, DC, 1990, pp. 398–413.
Oelkers, E.H., Schott, J., Devidal, J.-L., 1994. The effect of aluminium, pH, and chemical affinity on the rates of aluminosilicate dissolution reactions. Geochim. Cosmochim. Acta 58, 2011–2024.
Oliva, P., Viers, J., Dupré, B., 2003. Chemical weathering in granitic environments. Chem. Geol. 202, 225–256.
Paces, T., 1978. Reversible control of aqueous aluminum and silicate during the irreversible evolution of natural waters. Geochim. Cosmochim. Acta 42, 1487–1493.
Pacheco, F.A.L., Alencoão, A.M.P., 2006. Role of fractures in weathering of solid rocks: narrowing the gap between experimental and natural weathering rates. J. Hydrol. 316, 248–265.
Pacheco, F.A.L., Van der Weijden, C.H., 1996. Contributions of water–rock interactions to the composition of groundwater in areas with sizeable anthropogenic input. A case study of the waters of the Fundão area, central Portugal. Water Resour. Res. 32, 3553–3570.
Pacheco, F.A.L., Van der Weijden, C.H., 2002. Mineral weathering rates calculated from spring water data. A case study in an area with intensive agriculture, the Morais massif, NE Portugal. Appl. Geochem. 17, 583–603.
Pacheco, F.A.L., Sousa Oliveira, A., Van der Weijden, A.J., Van der Weijden, C.H., 1999. Weathering, biomass production and groundwater chemistry in an area of dominant anthropogenic influence, the Chaves–Vila Pouca de Aguiar region, north of Portugal. *Water Air Soil Poll.*. 115, 481–512.
Padilla, A., Pulido-Bosh, A., Mangin, A., 1994. Relative importance of baseflow and quickflow from hydrographs of karst spring. Ground Water 32, 267–277.
Press, W.H., Flannery, B.P., Teukolsky, S.A., Vetterling, W.T., 1991. Numerical Recipes in Pascal. Cambridge University Press, Cambridge, Massachusetts.
Rasse, D.P., Franćois, L.M., Aubinet, M., Kowalski, A.S., Vande Walle, I., Laitat, E., Gérard, J.C., 2001. Modelling short-term CO_2 fluxes and long-term tree growth in temperate forests with ASPECTS. Ecol. Modell. 141, 35–52.
Rodhe, A., Killingtveit, A., 1997. Catchment hydrology. In: Saether, O.M., de Caritat, P. (Eds.), Geochemical Processes, Weathering and Groundwater Recharge in Catchments. A.A. Balkema, Rotterdam/Brookfield, pp. 77–107.
Roelandt, C., Godderis, Y., Bonnet, M.P., Sondag, F., 2010. Coupled modeling of biospheric and chemical weathering processes at the continental scale. Global Biogeochem. Cy. 24, 18.
Rosso, R., Enechi, B.La., Barbera, P., 1991. Fractal relation of mainstream length to catchment area in river networks. Water Resour. Res. 27, 381–387.
Roth, G., La Barbera, P., Greco, M., 1996. On the description of the basin effective drainage structure. J. Hydrol. 187 (1–2), 119–135.
Rueda, F., Moreno-Ostos, E., Armengol, J., 2006. The residence time of river water in reservoirs. Ecolog. Model. 191 (2), 260–274.
Rupp, D.E., Selker, J.S., 2005. Drainage of a horizontal Boussinesq aquifer with a power law hydraulic conductivity profile. Water Resour. Res. 41, W11422. doi:10.1029/2005WR004241.
Rupp, D.E., Selker, J.S., 2006. Drainage of a horizontal Boussinesq aquifer with a power law hydraulic conductivity profile. Water Resour. Res. 42, W12421. doi:10.1029/2006WR005080.
Schermerhorn, L.J.G., 1956. Igneous, Metamorphic and Ore Geology of the Castro d'Aire–São Pedro do Sul region (northern Portugal). Ph.D thesis, University of Amsterdam, 617pp.
Schuller, D.J., Rao, A.R., Jeong, G.D., 2001. Fractal characteristics of dense stream networks. J. Hydrol. 243, 1–16.
Schumm, S.A., 1956. Evolution of drainage systems and slopes in Badlands at Perth Amboy, New Jersey. Geol. Soc. Amer. Bull. 67, 597–646.
Snow, D.T., 1968. Rock fracture spacings, openings, and porosities. J. Soil Mech. 94, 73–91.
Soen, O.I., 1958. The Geology, Petrology and Ore Deposits of the Viseu Region, Northern Portugal. PhD thesis, University of Amsterdam, 179pp.
Steefel, C.I., Lasaga, A.C., 1992. Putting transport into water–rock interaction models. Geology 20, 680–684.
Steefel, C.I., Van Cappellen, P., 1990. A new kinetic approach to modeling water–rock interaction: the role of nucleation, precursors, and Oswald ripening. Geochim. Cosmochim. Acta 54, 2657–2677.
Strahler, A.N., 1952. Hypsometric (area-altitude) analysis of erosional topography. Geol. Soc. Am. Bull. 63, 1117–1142.
Strahler, A.N., 1957. Quantitative analysis of watershed geomorphology. Trans. Am. Geophys. Union 8 (6), 913–920.
Szilagyi, J., Parlange, M.B., 1999. A geomorphology-based semi-distributed watershed model. Adv. Water Resour. 23, 177–187.
Szilagyi, J., Parlange, M.B., Albertson, J.D., 1998. Recession flow analysis for aquifer parameter determination. Water Resour. Res. 34 (7), 1851–1857.
Tarboton, D.G., 1996. Fractal river networks, Horton's laws and Tokunaga cyclicity. J. Hydrol. 187, 105–117.
Tardy, Y., Bustillo, V., Boeglin, J., 2004. Geochemistry applied to the watershed survey: hydrograph separation, erosion and soil dynamics. A case study: the basin of the Niger River, Africa. Appl. Geochem. 19, 469–518.
Van de Giesen, N.C., Steenhuis, T.S., Parlange, J.-Y., 2005. Short- and long-time behavior of aquifer drainage after slow and sudden recharge according to the linearized Laplace equation. Adv. Water Resour. 28, 1122–1132.
Van der Weijden, C.H., Pacheco, F.A.L., 2006. Hydrogeochemistry in the Vouga River basin (central Portugal): pollution and chemical weathering. Appl. Geochem. 21, 580–613.
Velbel, M.A., 1985. Geochemical mass balances and weathering rates in forested watersheds of the Southern Blue Ridge. Am. J. Sci. 285, 904–930.
Velbel, M.A., 1989. Effect of chemical affinity on feldspar hydrolysis rates in two natural weathering systems. Chem. Geol. 78, 245–253.
Velbel, M.A., 1993. Constancy of silicate–mineral weathering-rate ratios between natural and experimental weathering: implications for hydraulic control of differences in absolute rates. Chem. Geol. 105, 89–99.
Violette, A., Goddéris, Y., Maréchal, J., Riotte, J., Oliva, P., Kumar, M.S.M., Sekhar, M., Braun, J., 2010. Modelling the chemical weathering fluxes at the

watershed scale in the Tropics (Mule Hole, South India): Relative contribution of the smectite/kaolinite assemblage versus primary minerals. Chem. Geol. 277, 42–60.
White, A.F., 2002. Determining mineral weathering rates based on solid and solute weathering gradients and velocities: application to biotite weathering in saprolites. Chem. Geol. 190, 69–89.
White, A.F., Brantley, S.L., 2003. The effect of time on the weathering of silicate minerals: why do weathering rates differ in the laboratory and field? Chem. Geol. 202, 479–506.
White, A.F., Peterson, M., 1990a. The role of reactive surface areas in chemical weathering. Chem. Geol. 84, 334–336.
White, A.F., Peterson, M. (1990b). Role of reactive-surface-area characterization in geochemical kinetic models. In: Melchior, D.C., Bassett, R.L. (Eds.). Chemical Modelling of Aquous Systems II. ACS Symposium Series 416. Am. Chem. Soc., Washington, DC. pp. 459–475.
White, A.F., Bullen, T.D., Schulz, M.S., Blum, A.E., Huntington, T.G., Peters, N.E., 2001. Differential rates of feldspar weathering in granitic regoliths. Geochim. Cosmochim. Acta 65, 847–869.
Zhang, L., Lüttge, A., 2009. Theoretical approach to evaluating plagioclase dissolution mechanisms. Geochim. Cosmochim. Acta 73, 2832–2849.
Zecharias, Y.B., Brutsaert, W., 1985. Ground surface slope as a basin scale parameter. Water Resour. Res. 21, 1895–1902.
Zecharias, Y.B., Brutsaert, W., 1998. Recession characteristics of groundwater outflow and base flow from mountainous watersheds. Water Resour. Res. 24, 1651–1658.